CHAPTER 24
HF OVER-THE-HORIZON RADAR*

J. M. Headrick
Naval Research Laboratory

24.1 INTRODUCTION

Beyond-the-horizon ranges up to thousands of nautical miles can be achieved by radar operation in the high-frequency (HF) band (3 to 30 MHz). The longer-range performance is achieved by using sky-wave propagation. Ground-wave propagation over the sea is useful for short but still over-the-horizon distances. HF radar development over the past several decades has led to this capability,[1,2] and several operational systems are deployed.[3,4,5] Targets of interest are the same as for microwave radar and include aircraft, missiles, and ships. The wavelengths used are of the same order as ocean gravity waves, and this correspondence makes HF radar able to provide information on the waveheight directional spectrum and, by inference, surface winds and ocean currents.[6] In addition, this sensor is useful for observing various forms of high-altitude atmospheric ionization such as that due to aurora, meteors, and missile launches.[7,8] The wavelengths used and the nature of the transmission path make the spatial resolution coarse when compared with much-higher-frequency radars; however, the doppler resolution can be fine.

For effective radar operation, environmental parameters need to be determined in real time; transmission-path information is generally derived from adjunct vertical and oblique sounders as well as by using the radar itself as a sounder. An ionospheric electron-density model complex enough to enable adequate sounding interpretation is required. Ionospheric or transmission-path statistical forecasts are necessary for radar design and for development of the model, not for real-time operation. In addition, other users in the spectrum must be observed continuously and operating frequencies selected to avoid interference. In the context of transmission-path assessments for frequency selection, real time is measured as that interval in which there are no important changes in the ionosphere.

The magnitude and doppler distribution of the earth-surface backscatter is a major factor in setting system dynamic-range and signal-processing characteristics. Backscatter from the sea can be employed as a reference level and is a generally used diagnostic tool.

Figure 24.1 provides examples of radar coverage and spatial resolution appro-

* The comments, discussions and contributions by NRL colleagues J. Hudnall, J. McGeogh, R. Pilon, G. Skaggs, and J. Thomason are gratefully acknowledged.

priate for aircraft and ship targets. In the upper left the ray-path sketch shows that at higher-elevation radiation angles the rays escape, causing a skip zone of range coverage, that energy is returned to the earth until the reflection height horizon is reached, and that useful range coverage will lie between these limits. Although only one hop is shown, a multiplicity will exist, and energy may at times circle the earth. In the upper-right sketch, the ray paths show that different range extents are illuminated by using different operating frequencies, the longer ranges requiring the higher frequencies. In the example, 500 nmi is shown as the range coverage extent illuminated by one operating frequency. The trailing edge of an extent may vary as a function of radar parameters and target size, but the start is set by frequency selection and immediately follows the skip zone. Directly below is a plan view of the coverage area. It shows nine different areas that might be illuminated by a separate transmit beam of 8° width. It is likely that the ionosphere will vary across the 64° azimuth scan, so that if a single operating frequency is used, the range to the transmitter footprint will change with azimuth; however, in general a different operating frequency could be selected for each 8° to obtain the desired illumination. Each transmitter footprint is filled by 16 contiguous receive beams, each ½° wide. At the lower left, one illumination sector is shown divided into receive resolution cells with each cell being approximately 10 nmi on the side.

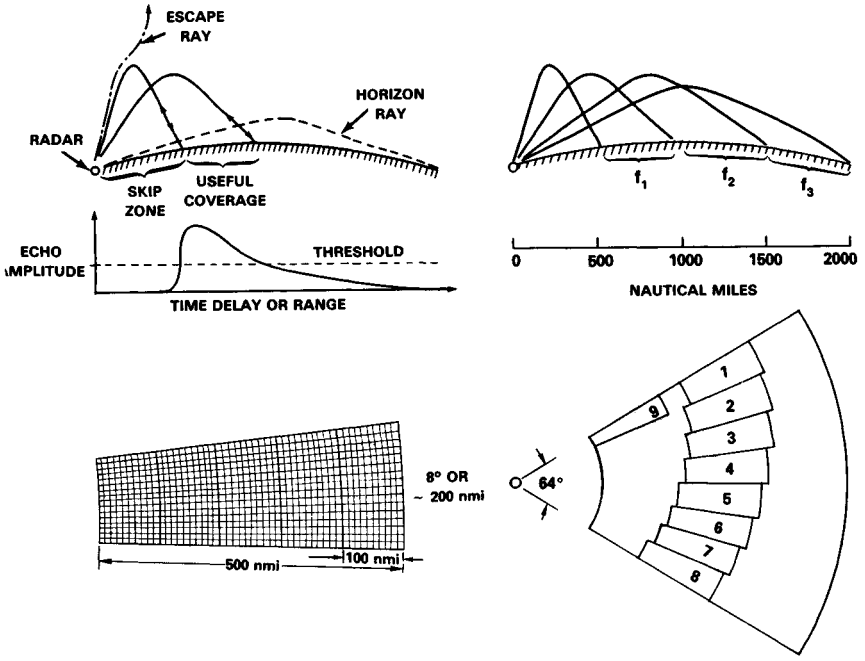

FIG. 24.1 At the upper left an example of single-hop sky-wave propagation with the useful coverage in range is sketched. On the upper right extended range coverage is obtained by using three frequencies. An azimuthal scan is shown in plan at the lower right, and at the lower left are given the receiver resolution cells in one transmitter footprint.

24.2 RADAR EQUATION

A form of the radar equation, Eq. (24.1), can be used to point to aspects of HF radar that are significantly different from radars that use higher frequencies. These differences include adaptation to environment, frequency and waveform selection, radar cross section, path losses, multipath effects, noise, interference, antenna gain, spatial resolution, and sky clutter.

$$\frac{S}{N} = \frac{P_{av} G_t G_r T \lambda^2 \sigma F_p}{N_o L (4\pi)^3 R^4} \tag{24.1}$$

where S/N = output signal-to-noise ratio
P_{av} = average transmitted power, W
G_t = transmitter antenna gain
G_r = receiver antenna gain
T = effective processing time, s
λ = wavelength
σ = target radar cross section
F_p = propagation-path factor
N_o = noise power per hertz
L = transmission-path and system losses
R = distance between radar and target

These parameters are explained as follows:

1. *Antennas, G_t and G_r:* A common convention for HF-band radars is to include earth effects in the antenna performance characterization, and that convention will be used here. For example, a half-wave dipole in free space has a maximum gain over an isotrope of 2.15 dB. If that antenna is oriented vertically, just above but not touching a perfectly conducting earth, its maximum gain will be increased by a factor of 4, or 6 dB, to 8.15 dB at 0° elevation angle. Since the earth is never perfect, its conductivity and dielectric constant are factors in determining antenna performance. The electrical properties of the earth are a much stronger factor for vertical polarization than for horizontal; however, terrain features and surface roughness are important for both polarizations.

2. *Coherent processing time, T:* HF radar is generally a look-down type that has earth backscatter at the same ranges as targets. Doppler processing is used to separate targets from earth backscatter.

3. *Wavelength (λ):* The wavelength or operating frequency must be selected so that energy is refracted by the ionosphere to illuminate the desired area of the earth. The spectrum of the emissions must be constrained not to interfere with other users. Since both the ionosphere and the HF-band occupancy distributions are time-varying parameters, adaptive radar management is required.

4. *Radar cross section (RCS), σ:* The radar cross section of conventional targets will generally be a function of frequency, polarization, and aspect angle. Often some sort of average value is used in analysis. Clutter levels will be large rel-

ative to most targets and therefore are important in radar design. For the RCS of earth clutter, the surface scattering coefficient σ^0 is multiplied by the resolution cell size A and the cosine of the grazing angle. The important resolution cell size factors, receiver antenna beamwidth and spectral bandwidth, are not explicitly contained in Eq. (24.1)

5. *Propagation factors (F_p):* Several propagation phenomena, including Faraday polarization rotation, multipath, and ionospheric focusing, may need inclusion in the equation. With linearly polarized radiation, Faraday rotation will result in a polarization mismatch varying with time and distance. That is, the target-incident-energy polarization will rotate as distance changes. Since many targets have RCSs that vary with polarization, an important result is that the most favorable polarization will illuminate the target recurrently.

6. *Noise (N_0):* For radars operating in the HF band it is possible to design antennas and receivers with low enough noise figures that environmental noise is dominant.

7. *Losses (L):* The loss term contains the two-way losses along the path traversed including ionospheric absorption and ground-reflection losses as well as any radar system losses. Ionospheric losses, while predicted on a statistical basis, constitute a major unknown in real-time radar operation.

8. *Range (R):* The range in the equation is the distance along the virtual path between target and radar. The ionospheric reflection height needs to be used to convert this range to great-circle ground distance. The apparent range to a particular target may take on more than one value since multiple paths may exist.

24.3 TRANSMITTERS

Most of the radar designs and missions require transmitter average power levels between 10 kW and 1 MW. Antennas are generally arrays of elements, and the common trend is to drive each element with a separate amplifier. This approach permits beam steering at a low level in the amplifier chain. Power control and amplitude-shaping requirements indicate a linear amplifier design. Since the radar uses doppler filter signal processing to separate the targets from the clutter, the clutter returned on the phase and amplitude noise sidebands radiated by the transmitter should be below that of desired targets. This can put a stringent condition on the emitted signal-to-noise ratio of the transmitter. The signal-to-noise ratio of the initial signal synthesizer must meet the requirements. The lower-level signal amplification can generally be designed to add no noise. Mechanical vibration in the high-power amplifiers can add noise, and care must be exercised in the air or liquid coolant flow system design.

The active element in each final transmitter stage can be either a traditional vacuum tube[9] or a solid-state device.[10] If the radar is to perform wide-area surveillance, frequent frequency changes are required in order to cover the various range extents. In addition, relative phase or time-delay changes are required in each amplifier chain to accomplish azimuthal steering. Reference 11 contains a discussion on modern high-efficiency amplifier designs for broadcasting; while some of the techniques are useful in radar transmitters, the final amplifiers tend to be narrowband. A broad-bandwidth performance and a tolerance to a variable standing-wave ratio load are desired features in a wide-area surveillance radar. Since the antenna elements will be wideband,

harmonic filters may be required. As an example, one transmitter and harmonic filter combination might have a 5- to 9-MHz passband and a stopband for 10 Mhz and higher frequencies; a second combination might pass up to 17 MHz and reject 18 Mhz and higher, and the design would continue in this manner to the highest frequency of operation.

24.4 ANTENNAS

A single antenna can be duplexed and used for both transmit and receive. The Naval Research Laboratory (NRL) magnetic-drum recording equipment (MADRE) antenna is an example.[1] This 100-m-wide by 40-m-high aperture provided sufficient gain and angular resolution for aircraft tracking in the upper part of the HF band: the frequencies used in daytime. A horizontal aperture of twice the width would provide similar resolution at night, where frequencies would be in the lower part of the HF band. However, it is desirable to have better azimuthal resolution for location accuracy and to reduce the clutter amplitude, and horizontal apertures of 3 km and even wider can be useful.[12,13] It is common practice to use separate transmit and receive antennas with the transmitter floodlighting many simultaneously formed receive beams. In elevation, desirable radiation angles run between 0 and 40°, with the specific angles depending on range and reflection height. Any sensitivity gained by directivity in elevation directly improves radar performance. This is in contrast with azimuth directivity for transmitting, where an increase in gain is accompanied by a decrease in area coverage. The AN/FPS 118 over-the-horizon (OTH) radar[3] does not employ steerable directivity in elevation but covers all necessary radiation angles with one broad elevation beam. This choice permits the antenna to have a relatively small vertical dimension. The AN/FPS 118 radar module uses a nominal 7.5° transmitter footprint filled with five receive beams; this combination is stepped as a surveillance barrier within a potential coverage area 500 to 1800 nmi in distance by 60° in width.

The antennas and power amplifiers used in HF broadcast station service have much in common with an HF radar transmitter-antenna combination; that is, the broadcast-service aim is to obtain a specified level of illumination over some selected area. The multiple-band and steerable broadcast antennas reviewed in the *IEEE Transactions on Broadcasting* Special Issue on Short-Wave Broadcasting,[11] those described in Johnson and Jasik,[14] pages 26–29 through 26–35, and those given in "Shortwave Antennas,"[15] Chaps. 13 and 14, are examples. It will be noticed that many of the broadcast-service antennas employ large vertical apertures. However, antennas used for radar have an added severe demand to minimize mechanical motion that would cause signal modulation, and this requirement is easier to meet with low-antenna-height designs.

Among the many factors that influence antenna design are:

1. The transmitter-receiver antenna gain product must be large enough to make its required contribution to sensitivity.

2. The receive beamwidth must be narrow enough to provide the required location accuracy.

3. The receive beamwidth must restrict clutter levels to values permitted by system dynamic range and slow-target detection requirements.

24.5 CLUTTER: THE ECHO FROM THE EARTH

Early in HF radar experiments it was noted that the clutter received by sky-wave paths represented a large signal and provided an indication of the earth-surface area illumination. Extensive observations made at the Naval Research Laboratory viewing alternately Atlantic Ocean areas and central United States areas indicated that, averaged over a wide area, sea clutter power levels were about an order of magnitude higher than those from an area of similar size in the central United States. Later observations indicated even less backscatter from ice-covered Greenland areas. The backscattered energy from land is topography-dependent; as an example, a city in the central plains provides a larger echo than its surroundings. In contrast with such abrupt changes, the seascattering coefficient σ^0 for HF radio waves is fairly uniform; that is, it changes gradually with range and azimuth. The sea echo power is proportional to the resolution cell area, to a good approximation. The nature of the sea echo needs some description. For the seascattering coefficient to be approximately constant, long time averaging (minutes) is required. Sky-wave transmission characteristics are notably variable; however, the sea echo can be used as an amplitude reference when care is exercised. An elementary description of sea echo behavior and some applications follows.

Ocean wave generation and propagation are a complex and not completely understood subject; a similar statement can be made about electromagnetic scattering from the waves. However, for the scale size of HF-band wavelengths the sea is a surface that is only slightly rough, and the method of Rice[16] can be used to explain reflection. Backscatter from the sea can be considered a resonant interaction. The disorganized-looking ocean waves are thought as being the sum of an infinite number of Fourier surfaces, each being a sinusoidally corrugated sheet with a different wavenumber and direction.[17] The principal backscatter for a grazing-incidence electromagnetic wave comes from that component sheet that has a wavelength equal to one-half of the radar wavelength and that is either directly approaching the radar or receding from it.[18,19] The surface scattering coefficient, or RCS per unit surface area (σ^0), is much larger for vertical than for horizontal polarization. The echo from the sea with horizontal polarization can be neglected at the smaller grazing angles. The water wavelengths between 10 and 100 m are gravity waves that in deep water follow the dispersive relation

$$v = \left[\frac{gL}{2\pi}\right]^{1/2} \tag{24.2}$$

where v = water-wave phase velocity
g = acceleration of gravity
L = water wavelength

Ocean waves are excited by the surface winds. If a wind blows at a constant velocity long enough and over sufficient fetch, a steady-state condition will be achieved where the wind provides just enough energy to the water to supply that lost in breaking and other dissipation. It will completely arouse the water waves with a phase velocity nearly equal to the wind speed. It will also completely arouse all the ocean waves of lower velocities. Figure 24.2*a* gives an example of the spectrum as derived from a measurement of waveheight versus time at a particular point. Pierson and Moskowitz have derived the following relation for a fully developed spectrum based upon empirical data.[20]

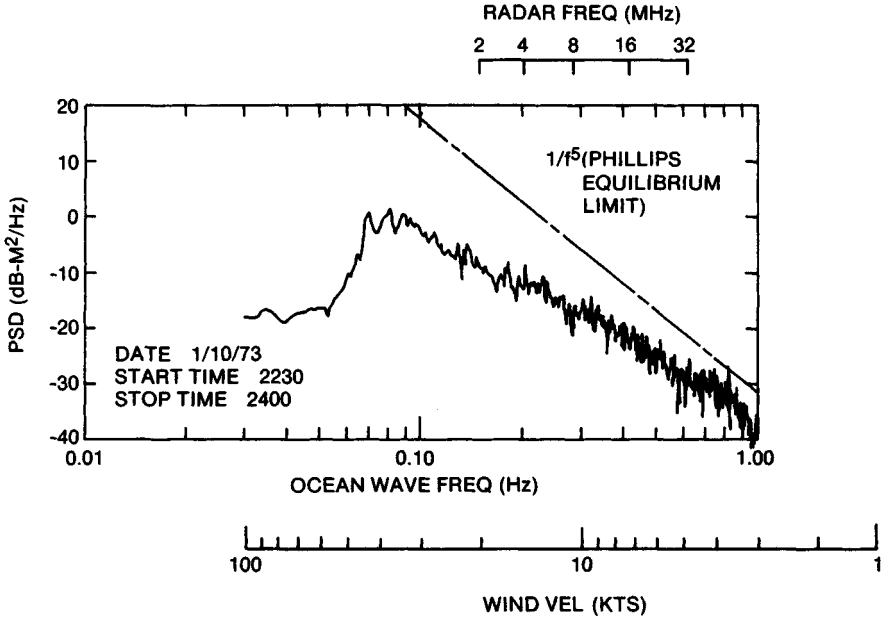

(a)

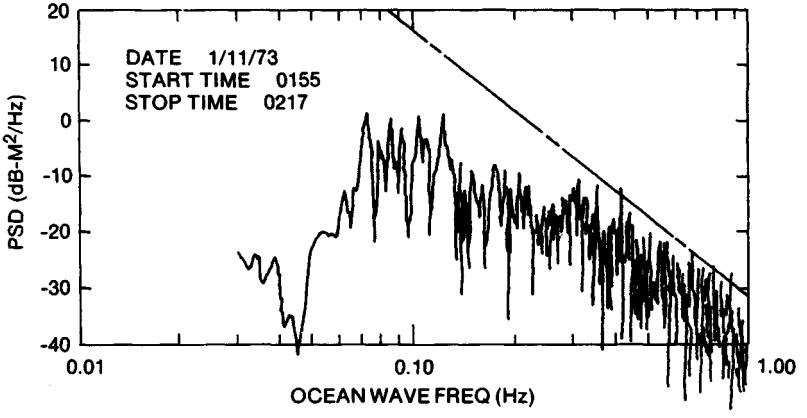

(b)

FIG. 24.2 (*a*) Ocean-waveheight power spectral density (PSD) is given as a function of water-wave frequency. The straight line is a saturation asymptote, and for this example the limit is approached at the higher frequencies. The scale marked "wind velocity" can be used to deduce that winds up to 40 kn have excited waves with frequencies as low as 0.08 Hz but that either the length of time or the fetch, or both, have not been sufficient for full development. In this example the individual spectral analyses, requiring about 100 s of data, have been averaged for 1½ h. (*b*) The spectral density is given as in *a* but is averaged over a shorter time, 23 min. Both higher peaks and deeper voids are seen. The scale across the top of *a* gives the radar operating frequency that experiences resonant backscatter, and it can be seen that at many frequencies this level is far below the long-term average.

$$S(\omega) = C_1 g^2 \omega^{-5} \exp\left[-C_2\left(\frac{g}{\omega v}\right)^4\right] \tag{24.3}$$

where S = waveheight squared per hertz
ω = water-wave angular frequency
v = wind speed
C_1, C_2 = constants

The exponential term approximates the decay in the spectrum above the wind maximum velocity. The ω^{-5} asymptotic term is a feature of major interest and use. This saturation effect suggests that the sea echo can provide an amplitude reference, and an important consequence is that with such a reference path losses may be estimated. The inference is that for vertically polarized waves from a radar, looking along the wind direction, σ^0 is constant for a specific radar operating frequency if the sea is fully developed. Further, following the analysis of Barrick,[19] σ^0 will have the same value for all water-wave frequencies along the wind direction where the sea is fully developed. In general, the scattering coefficient will be proportional to the resonant waveheight squared. The term *resonant* refers to the Fourier component of the surface where the water wavelength multiplied by the cosine of the grazing angle equals one-half of the radar wavelength. This type of scatter is frequently refered to as *Bragg scatter*. These models are helpful in developing an understanding of the sea surface and the radiowave interaction; however, a very long time average is implied when the water-wave spectrum is described as the product of two terms, one of which is frequency to the minus fifth power and the other an exponential with frequency in the argument. A single 100-s look at the waveheight-squared spectrum with a frequency resolution of $\frac{1}{100}$ Hz would yield a very jagged spectrum; Fig. 24.2*b* provides a short look to contrast with the long time average of Fig. 24.2*a*.

The variability and value of $\sigma_{vv}{}^0$ was examined with the San Clemente Island ground-wave radar.[21] The *vv* subscripts indicate that both transmission and reception were vertically polarized. This radar had several valuable and unique features: a transmission path out over the open sea, multiple-frequency operation in a repetition period, calibrated antennas, known transmitter power, and ground truth in the form of ocean-waveheight recordings. When looking into an approximately 20-kn wind, values of $\sigma_{vv}{}^0$ were found to be constant within a few decibels for operating frequencies where the water-wave spectrum was approximately fully developed; these observations provided a confirmation of Barrick's first-order theory.[19] It is emphasized that a constant level in scattering coefficient implies long averaging times. By using the antenna gain conventions stated earlier and a semi-isotropic sea directional spectrum, the value of $\sigma_{vv}{}^0$ was calculated as -29 dB, and the measured values were grouped between -7 and $+3$ dB of this value over a 5- to 20-MHz-frequency span. This experiment provided a direct measure of the sea-surface scattering coefficient and has exposed characteristics that should be considered when using σ^0 as a reference.

Some other features need consideration. Water-wave directions neither will be confined to the wind direction nor will they be semi-isotropic, but they will spread throughout 360°, with the spreading function depending upon frequency and other variables. Oceanographers generally treat the directional wave spectrum in the wind direction half plane only.[22] But HF radar has sufficient sensitivity to expose the waves running against the wind that have an RCS more than two orders of magnitude below those running with the wind. If the wave directional-spectrum distribution of Long and Trizna is used, the maximum value

of σ^0 for a saturated sea is -27 dB in the upwind or downwind direction (longitudinal sea) and is -39 dB in the crosswind direction (transverse sea).[23] Figure 24.3 gives the nominal shape of the scattering coefficient for these two conditions. The statements so far have all related to vertical polarization, which will have the largest scattering coefficient. Sky-wave radar resolution cell sizes are generally large enough that Faraday rotation can be expected to cause illumination of a resolution cell to be over all polarization angles and consequently to reduce the average value of σ^0 by 3 or 4 dB, depending on the elevation radiation angle. If -30 dB is used for the effective scattering coefficient and a resolution cell is considered to be a square 10 nmi on a side, the surface area A is 85 dBsm and the RCS is $85 - 30 = 55$ dBsm. A 12 dB path enhancement will be effective owing to constructive multipath addition, which will increase the resolution cell effective RCS to 67 dBsm. The receiver and processor must be able to handle both the high-level signal due to this large RCS and those much smaller signals due to targets. An HF radar must be designed to accommodate such clutter levels even though they will not exist all the time or at any one time over all areas, especially at the lower operating frequencies.

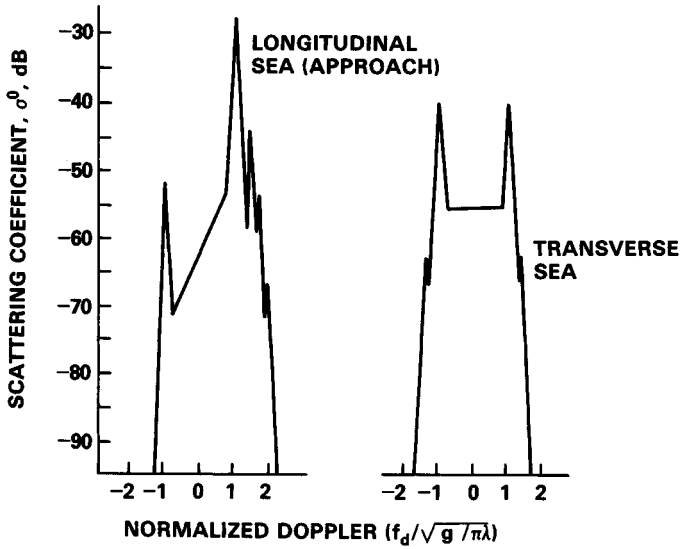

FIG. 24.3 The nominal maximum values of the seascattering coefficient are given as a function of doppler frequency for a coherent processing time of 51 s. A longitudinal, directly approaching or receding sea gives the largest value. A transverse, cross to the radar look direction, gives two peaks equal in height.

By scanning over a radar's total potential coverage area and using the ratio of the two resonant doppler frequency sea responses, a map of sea principal direction can be constructed.[23,24] By inference, surface winds can be mapped. Surface-wind maps are a regular contribution by the Jindalee radar.[25] Actual waveheight estimates can be made on the basis of the multiple scatter features of the sea echo spectra.[21,24,26–28] A major difficulty with these methods lies in eliminating corruption of the echo doppler spectrum by ionospheric path propagation.

Trizna has reported a method for estimating σ^0 from three simple and direct measurements made on the radar echo spectrum, and this method is relatively insensitive to propagation-path variation.[29,30] All the methods for estimating sea state or scattering coefficient require long coherent processing times plus incoherent averaging of a number of coherent times in order to achieve a distinct and repeatable amplitude-doppler signature. This type of radar operation will frequently be incompatible with other radar missions. However, the sea echo is a large signal, and it can be obtained with an adjunct oblique sounder operating in an appropriate radar mode.

In summary, the sea echo power in a resolution cell (1) is generally the largest in-band echo signal; (2) generally exists in the open ocean even in relative calm; (3) varies as the square of resonant waveheight, which is frequently limiting at the higher frequencies; and (4) varies with direction, being greatest for seas running toward or away from the radar.

24.6 RADAR CROSS SECTION

The RCS of the sea has been treated in Sec. 24.5. A number of natural scatterers have been described at the 1981 Symposium on the Effect of the Ionosphere on Radiowave Systems.[31] Findings on the nature of auroral echoes are given by Greenwald,[8] and an auroral echo-scattering model has been developed by Elkins.[32] Chapter 4 of Ref. 7 treats the RCS associated with rockets and their exhausts. Here attention will be confined to echoes from airborne and surface targets.

Aircraft and ships have dimensions that put them in the resonant scattering region. The smallest aircraft and cruise missiles will be in the Rayleigh scattering region for the lower half of the HF band. The RCS has aspect sensitivity but strongly depends upon the target's gross dimensions. For an aircraft the span of the wings, the fuselage length, the tail and elevator span, the vertical stabilizer and rudder height, and their relative locations are the features that determine the RCS. Target shaping of a scale size much less than a wavelength will have little effect. For bodies with high-conductivity surfaces the scattering cross section can be calculated by using numerical methods.[33] Facilities exist where good scale-model measurements can be made, and the Ohio State University compact range is an example.[34]

Rough but useful RCS estimates can be made by using the behavior of a few "canonical" shapes. Figure 24.4 is a family of plots giving RCS versus radar frequency for an oblong-shaped conducting body. The straight line marked 90° $\lambda/2$ dipole gives the RCS of a resonant, conducting half-wavelength rod, where the rod is parallel with the electric field. This geometry gives the maximum RCS for the rod. The upper scale of the abscissa gives the one-half-wavelength dimension of the frequency given on the lower scale. The curve marked 90° is the RCS of the oblong-shaped conducting body of 11-m length and 1-m thickness; again the target long dimension is aligned with the electric field. The maximum RCS coincides with the nominal half-wavelength dimension or with the first resonance. The curves marked 45, 15, and 0° give the RCS as the target is rotated to these angles in the plane that contains the electric vector. The little sketches give, at the left, the body shape, then the RCS patterns at nominal ½ wavelength, 1 wavelength, and ½ wavelength in order to help visualize how the RCS will change as the as-

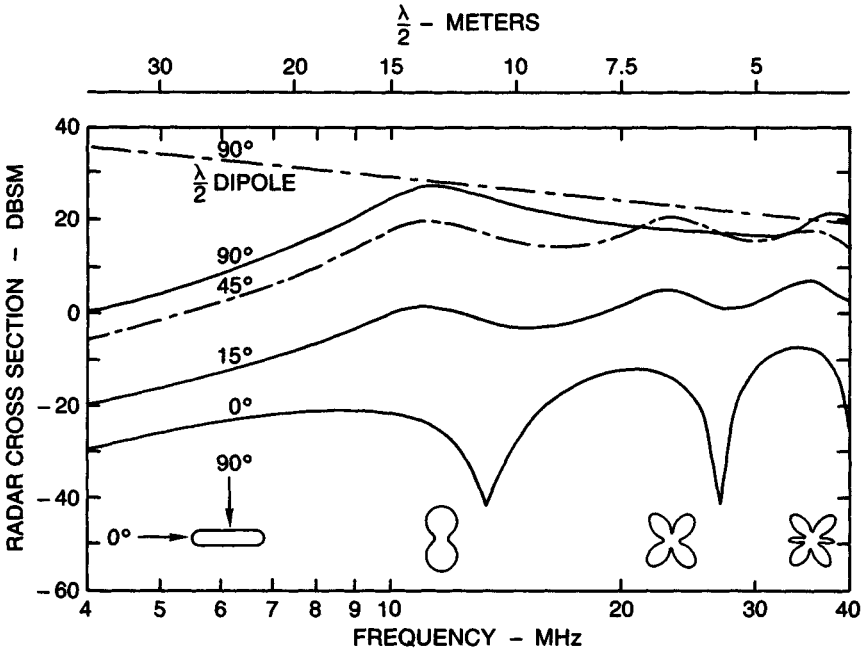

FIG. 24.4 The RCS is given versus frequency for an 11-m-long and 1-m-thick oblong conducting target. The *E* vector and the 11-m dimension are in the same plane; 0° (nose-on), 15°, 45°, and 90° (broadside) curves are given. The top dashed curve is for a resonant dipole at 90°. The little sketches at the first, second, and third resonances of the 11- by 1-m target show how the RCS behaves with an illumination aspect.

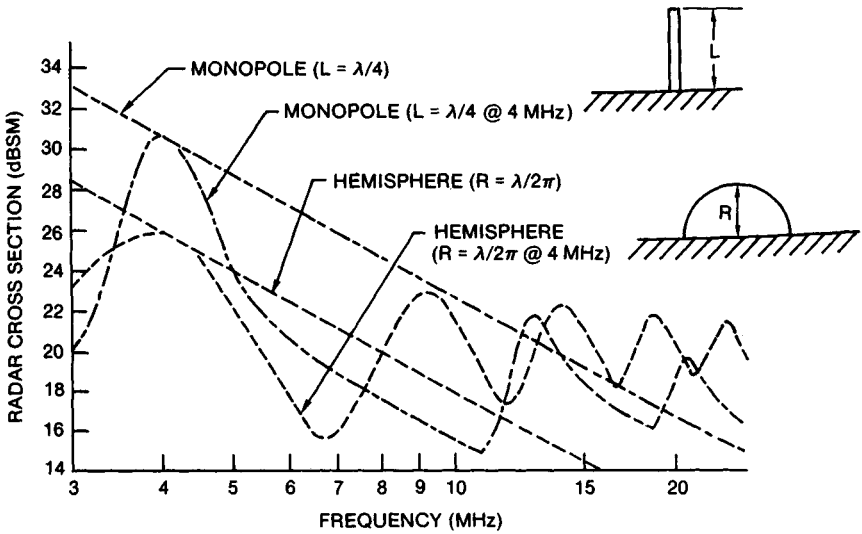

FIG. 24.5 The vertical-polarization RCS of a hemisphere and a monopole on a perfect conductor are plotted against the radar operating frequency.

pect angle is varied. For targets of other lengths with approximately the same shape factor, the response can be determined by sliding the curve along the $\lambda/2$ line and making the first resonance coincide with the line at the ½-wavelength point. Aircraft with their wing-fuselage cruciform shape will have an RCS that varies with the aspect angle but not greatly. As has been mentioned, Faraday rotation will ensure periodic illumination with the most favorable polarization.

Figure 24.5 gives the vertical-polarization RCS of a rod and a hemisphere sticking out of a perfectly conducting surface. With these canonical shapes an estimate of RCS can be made for surface craft. For small vessels the mast height will be of most importance.[35] For surface targets where the maximum RCS is with vertical polarization, the 12 dB sky-wave RCS enhancement mentioned for the sea echo will occur.

24.7 NOISE AND INTERFERENCE

In the HF band, receiving systems can be designed such that external noise is dominant. The major source of noise at the lower frequencies is lightning discharges ionospherically propagated from all over the world (*sferics*). At the high end of the band, extraterrestrial or galactic noise may be larger than that due to sferics. Receive sites in an area of extensive electrical equipment use can find human-made noise dominant. The HF band is well occupied by other users, and channel selection can be such that other transmitter emissions constitute the background "noise" level.

The widely used source on noise is International Radio Consultative Committee (CCIR) Report 322.[36] This report is based upon measurements made at 16 locations throughout the world. The measurement and data analysis was performed to exclude individual collection site local thunderstorm contributions. Spaulding and Washburn[37] have added data from the U.S.S.R., and a revised CCIR report is available. The noise-level medians as a function of frequency are given in the form of worldwide maps by season and 4-h time block. Lucas and Harper[38] have provided a numerical representation of CCIR Report 322 useful for computer computations, and this has been revised by adding the work of Spaulding and Washburn. The numerical maps of median values are accompanied with decile values to indicate distributions over days of the season. These noise maps provide the level that an omnidirectional antenna would receive. The common method of use is to treat the noise as isotropic even though it must be azimuth- and elevation-angle-dependent. Examination of maps indicates that tropical rain forests and other regions of concentrated thunderstorm activity are major sources of noise. Also, examination suggests that a denser distribution of data collection sites would improve the data. It would be very useful to have noise source maps so that antenna patterns and explicit propagation effects could be taken into account. Some work toward source maps has been done by Ortenburger and Kramer,[39] but there is no known generally available database in this form.

Even though available noise description has limitations, it does provide a reference level for radar design. An HF radar is generally designed to take advantage of what the environment permits; that is, the receiver noise figure should be good enough to make environmental noise the limitation. An example of the CCIR Report 322 data will be discussed. Figure 24.6 was drawn from Lucas and Harper.[38] Noise power in a 1-Hz band relative to 1 W (dBW) is given as a func-

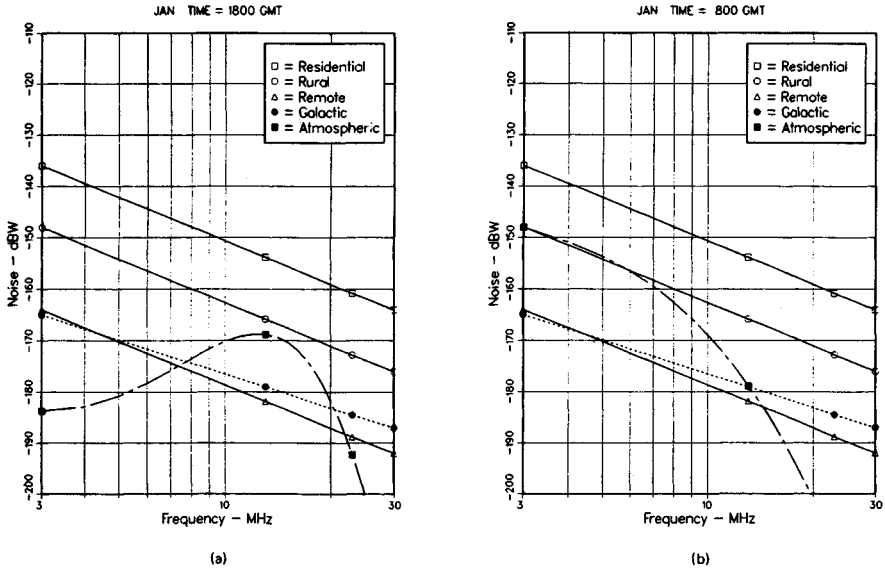

FIG. 24.6 Noise power per hertz is given for 38.65° north latitude and 76.53° west longitude and winter. (*a*) 1800 UTC is given as a daytime example. (*b*) 0800 UTC is given as a nighttime example. Universal time coordinated (UTC) and Greenwich mean time (GMT) are interchangeable in this treatment.

tion of frequency for three different sources of noise. The practice in use is to select the largest. This is a winter daytime example at a United States east coast location. The three straight lines are estimates of anthropogenic (formerly man-made) noise for three different types of sites. The shape of the anthropogenic curves is described by the equations

$$N_0 = -136 - 12.6 \ln (f/3) \quad \text{residential}$$
$$N_0 = -148 - 12.6 \ln (f/3) \quad \text{rural}$$
$$N_0 = -164 - 12.6 \ln (f/3) \quad \text{remote}$$

where the frequency f is in megahertz and ln indicates the natural logarithm. The above trends with frequency approximate many measurements of human-made noise; however, ideally the curve would be based on measurements at the particular radar site. The galactic-noise curve should be selected when it is the largest and when there is a path through the ionosphere; the path will not exist for the lower operating frequencies in the daytime. The atmospheric noise rises from low frequencies to about 12 MHz and then rapidly falls. Figure 24.6*b* is for nighttime. All the curves are the same as in Fig. 24.6*a* except for atmospheric noise. At 10 MHz the night and day levels are the same; below 10 MHz the noise decreases with decreasing frequency in daytime and increases at night. Above 10 MHz daytime levels are greater than those at night. These effects can be partially explained by the very lossy long-range paths in day that attenuate the long-range noise at the lower frequencies and by there being few or no sky-wave paths to noise terrestrial sources at the higher frequencies at night. Later it will be seen that in general nighttime noise will be greater than daytime noise for sky-wave

illumination of a selected range. The general trends of atmospheric noise in other seasons are similar to those of winter. However, there can be large differences in level at other locations on the earth.

Other effects that can control radar performance are sometimes mistaken for the *passive* noise discussed above. One of these is the spread-in-doppler clutter from localized high-density irregularities in sky ionization; this is sometimes refered to as *active* or multiplicative noise. The occurrence of this type of clutter is greater at night and is much more prevalent in the auroral zones and around the magnetic equator. As stated earlier, Elkins[32] has developed a model for HF auroral clutter that can be used to predict target obscuration when the transmission path is through the auroral region. Lucas has provided spread-F maps for inclusion in ionospheric models so that spread doppler clutter can be predicted.[40] Ionospheric irregularities that scatter back to the radar receiver occur much more often at night than by day at any latitude. Their effects can be reduced with spatial resolution.

Anyone engaged in extensive HF radar performance analyses should have the numerical description of noise maps in their computer data files. When only a few performance predictions are needed, CCIR Report 322 can be used manually.

24.8 SPECTRUM USE

The waveforms that can be effective for HF radar are in general similar to those used at the higher frequencies and are selected for similar reasons. However, the transmission path is dispersive, and waves experience polarization rotation with frequency; because of these effects, bandwidths are limited to the order of 100 kHz without correction. The more restrictive constraint on emissions is that of noninterference to and by other services.

Frequency spans in the HF spectrum are allocated for various types of service such as broadcasting, point-to-point communications, maritime mobile, aeronautical mobile, standard frequency and time, and amateur. The variability of the sky-wave transmission medium requires different operating frequencies at different times. A single point-to-point circuit can require as many as five different frequencies spread over a wide range if the circuit is to be reliable over all hours of the day and seasons of the year and through the solar activity cycle. If a radar is to perform surveillance over large areas by ionospheric refraction at all times of day, seasons, and degrees of solar activity, frequency channels distributed over a large part of the HF band are required, although only a single channel may be used at any one time. When the HF band is scanned with a spectrum analyzer at a particular hour, it can be seen that the gross features of occupancy are remarkably stationary over the days of a season. This is due to broadcast stations, fixed-service point-to-point transmitters, and many other spectrum users having regular schedules. Figure 24.7 examines one particular segment and time. These observations were made with 5-kHz-bandwidth filters. When narrower-bandwidth filters with steep skirts are used, several channels 5 to 10 kHz wide with no detectable users are generally found within any 1-MHz span. The maximum frequency that will still reflect energy back to the earth during the day may be twice that at night; therefore, the occupancy tends to be denser at night than during the day.

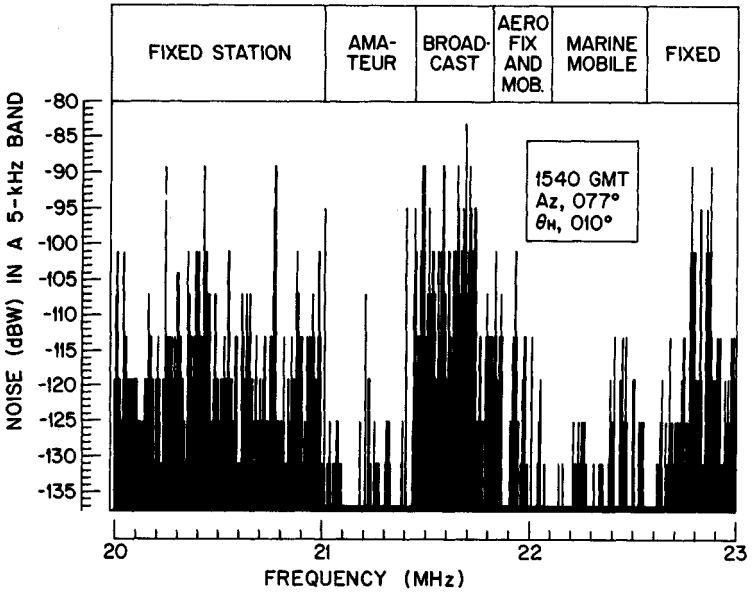

FIG. 24.7 An example of spectrum occupancy measured at the MADRE radar.

The part of the spectrum that is useful for sky-wave propagation is densely populated. Even out-of-band signal levels are a consideration in receiver front-end design, where it is convenient to have bandwidths much wider than that of the radar signal. There are a large number of broadcast stations that have 500-kW transmitters and antennas with more than 20-dB gain. Measurements made on the middle Atlantic coast of the United States show HF broadcast-band signals with strengths of 5 to 10 mV/m. These ambient levels must be accommodated in receiver design since a wideband front end is desirable for rapid and frequent frequency changes.

The practice in allocations for HF radar operation is to permit use of broad bands of the spectrum with a requirement to cause no interference to an existing service and to provide a lockout feature for channels that need protection. An integral part of an HF radar is a channel occupancy analyzer that provides a real-time description of spectrum availability.

24.9 SKY-WAVE TRANSMISSION MEDIUM

Solar radiation and particle emission bombardment are the cause of ionization in the earth's upper atmosphere. Even though there is no incident radiation at night, the ionization never completely decays; that is, there is always an ionosphere. The electron-density distribution is the major control over the propagation of HF radio waves. Ground illumination over the horizon is enabled by refraction in the ionosphere. When an oblique-incidence radio wave traverses a path where electron density is increasing with altitude, the ray is bent away from the vertical; if

the gradient in density is sufficient, the wave will "reflect" back back to the earth, providing long-distance illumination. The lower the radio-wave frequency, the smaller the required gradient. Since some ionization in the upper atmosphere always exists, it is always possible to illuminate the earth over the horizon if there is freedom in frequency selection. Ionospheric outages do not exist in the sense that long-distance illumination is impossible. Path outages are due to deficiencies in frequency channel allocations and insufficient radiated power. Additional factors that can affect radar performance are ionization irregularities that degrade path quality and backscatter from spread-in-doppler ionization gradients that can obscure targets.

The solar activity that drives the ionization of the earth's atmosphere is variable on a diurnal, seasonal, and long-term basis with a superimposed random component. Current prediction and analysis methods depend upon a statistical description of the ionosphere. A large amount of vertical-incidence reflection-height versus frequency-sounding (ionosonde) data has been collected over several decades, and from this data most descriptions of the ionosphere are derived. Davies[41] and Chap. 10 of the "Handbook of Geophysics and the Space Environment"[42] can be read for information on ionospheric radio-wave transmission. The radar designer needs a statistical description that will permit matching the design to the required frequency span, power levels, and vertical radiation-angle gain. The radar operator needs a model with enough sophistication to permit full interpretation of the real-time soundings for both operating parameter selection and data analysis.

The regions of the ionosphere that are considered necessary to model for an understanding of transmission paths are as follows:

1. *D region:* This region occupies the lowest altitudes considered. It ranges from 50 to 90 km, where electron density rapidly increases with altitude in the daytime. The maximum ionization in the D region occurs near the subsolar point and will be greatest during periods of highest solar activity (sunspot maximum). The D region may not be explicit in some ionospheric models where its effects are accounted for with an empirically derived path-loss calculation. Most models have this nondeviative absorption as a median value plus a distribution.

2. *E region:* This ionization region extends between about 90 and 130 km in altitude with a maximum near 110 km when sunlit. In addition, there may be anomalous ionization referred to as sporadic E. This latter ionization layer is thin in altitude, may be either smooth or patchy, is seasonally and diurnally variable but not well correlated with solar activity, and has marked variation with latitude.

3. *F Region:* This is the highest-altitude region of interest for sky-wave propagation, and it is also the region of greatest electron density. In the daylight hours there may be two components that should be recognized, especially in summer. The F1 region lies between 130 and 200 km and, like the E region, is directly dependent upon solar radiation; it reaches maximum intensity about 1 h after local noon. The F2 region is variable in both time and geographical location. The altitudes of the F2 region peaks are considered to lie between 250 and 350 km in the middle latitudes. The F2-region ionization shows marked day-to-day variations and in general is not the regular sun follower that the E and F1 regions are. Most models have a statistical description of F2 maximum electron density (or critical frequency) in the form of a median and upper and lower decile values.

Goodman and Reilly discuss shortwave prediction methodologies on pages 230 to 237 of Ref. 11. The ionospheric models that have been extensively used in

HF radar performance analysis are in programs called ITSA-1, ITS-78, RADAR C, IONCAP, and AMBCOM.[43–47] Lucas[48] provides some detail on these models and their origins. In summary, they all draw on the large database of recorded ionospheric soundings made during the International Geophysical Year of 1957–1958 and the International Year of the Quiet Sun of 1964–1965. All the models rely heavily on data taken from the maximum and minimum solar activity years of one solar cycle, with supplement from an adjacent cycle of lower activity. Linear interpolation between the two extremes is used for conditions of intermediate solar activity. This limited database might be considered a serious deficiency since there can be considerable difference in the measure of solar activity from one cycle to another. However, while the degree of atmospheric ionization appears to be a strong function of position in the solar cycle, it has only a weak dependence on solar activity measure. The commonly used indices or measures of solar activity are the sunspot number (SSN) and the radiated-microwave flux density. On a yearly average basis these indices relate well to the median ionospheric description; however, short-term predictions are more difficult to relate to solar activity. In general, the models listed are part of a prediction method. Some of the prediction methods have not been well documented although widely distributed; also, users frequently "improve" upon a model and prediction method to suit their specific needs. As an example, the model RADAR C of Ref. 45 is the basic building block of Thomason, Skaggs, and Lloyd in NRL Report 8321;[49] however, they have added a D region, a collision-frequency distribution, an earth's magnetic field, a topside electron distribution, an auroral electron-density modification,[50] and other features that make the model more generally useful. The ionospheric model as described in NRL Report 8321 will be used for examples here.

A form for display of the data is that of vertical virtual height versus frequency sounding and a true-height plot. *Virtual height* is defined as the speed of light times the time delay for the ionospheric echo; *true height* is the actual distance to reflection height. The critical frequency is the highest frequency that is reflected. Reference 46 has a figure that illustrates how the stored median ionosphere compares with a set of actual soundings; it is shown here as Fig. 24.8. Each of these soundings was made at the same hour but on a different day of the month. In this figure each trace shows the virtual height of a vertical sounding versus probing frequency for the ordinary ray. When vertical soundings are made with an ionosonde that uses a linearly polarized antenna, the ionosphere will be birefractive and provide two traces that are called *ordinary* and *extraordinary*. With right-hand and left-hand circularly polarized antennas the two responses can be separated. Figure 24.9*a* and *b* gives an example in the mid-Atlantic off the east coast from the data file. Such plots can be obtained at a selected earth location for a specified level of solar activity (SSN), month, and time of day. Similarly to the illustration given in Fig. 24.8, if a collection of experimental soundings is taken at the geographical location, SSN, and times of day of Fig. 24.9 over a month, the medians will approximate the curves of Fig. 24.9 closely. In addition, the upper and lower decile values of the measured monthly families of F2 critical frequencies will deviate from the median by about ±25 percent. For radar performance calculations median values will be used. However, when designing a radar, distribution should be considered for lowest operating-frequency selection. Distributions are important in communications when a limited number of channels are assigned, but since the radar operating practice is to select a near-optimum frequency, distribution is not important. The model uses three parabolas to approximate the electron distribution with altitude. Electron density and

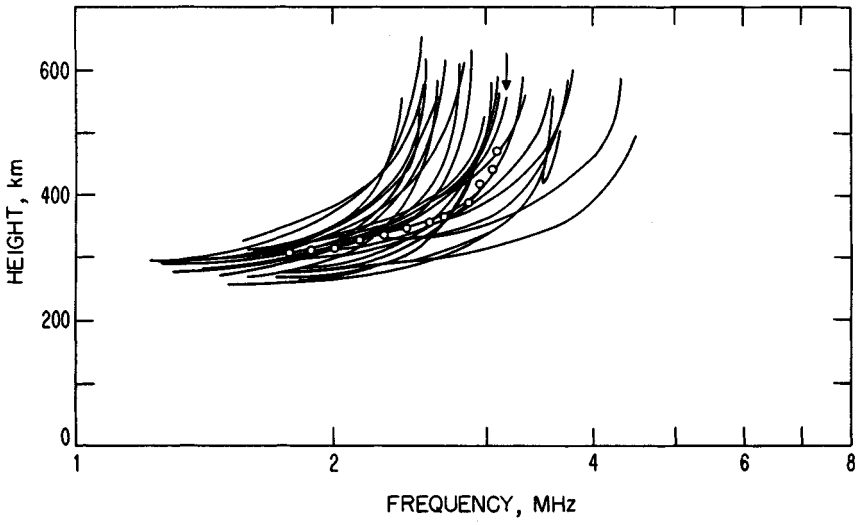

FIG. 24.8 A predicted vertical-incidence ionogram is compared with observed ionograms. The arrow points to the predicted 3.2-MHz critical frequency, and the little circles give points on the predicted median sounding. The measured median of this ensemble is about 3 MHz.

critical or plasma frequency are sometimes used almost interchangeably; when this occurs, the relation implied is $N_e = f^2/81$, where N_e is free-electron density, in numbers per cubic meter, and f is the frequency, in hertz. For the little tables shown in Figs. 24.9 and 24.10, FC is the critical frequency, in megahertz; HC is the height of maximum ionization or the nose of the parabola, in kilometers; and YM is the semithickness of the parabola, in kilometers. ES gives the sporadic-E distribution as M (median), L (lower), and U (upper) decile critical frequencies, in megahertz. This table shows the form of the stored data in the ionospheric model, and with it the various profiles can be generated. All these constants can be adjusted to fit diagnostic observations.

In Fig. 24.9 it is seen that the F2 critical is 6.5 MHz in the daytime and 4 MHz at night for summer. Figure 24.10 gives similar data but for winter, where the day and night comparison is from 8.4 MHz to 3.5 MHz. Figures 24.11 and 24.12 give summer and winter plasma-frequency contours for the same location versus time of day. These plots are provided to show how abrupt the night-to-day and day-to-night transitions are; during winter dawns the critical frequency changes from 2 to 5 MHz in 1 h. The radar-frequency management task is most difficult in these time periods; during most of the day and most of the night changes are relatively slow. This data indicates the median diurnal frequency variations required for a particular path: more than 2:1 in winter and somewhat less in summer. Day-to-day variability will impose greater extremes.

In this section the predictable and random variability of the transmission path has been indicated. When extensive and detailed radar performance calculations are to be made, a computer-stored base is required.

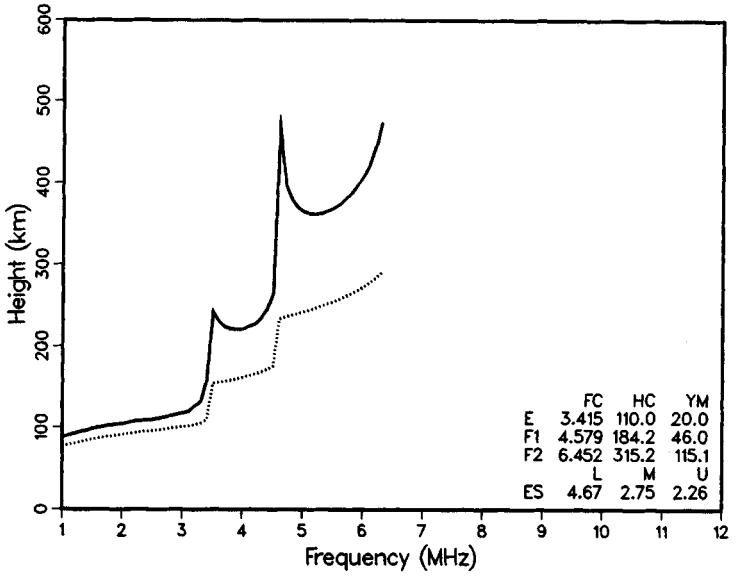

(a)

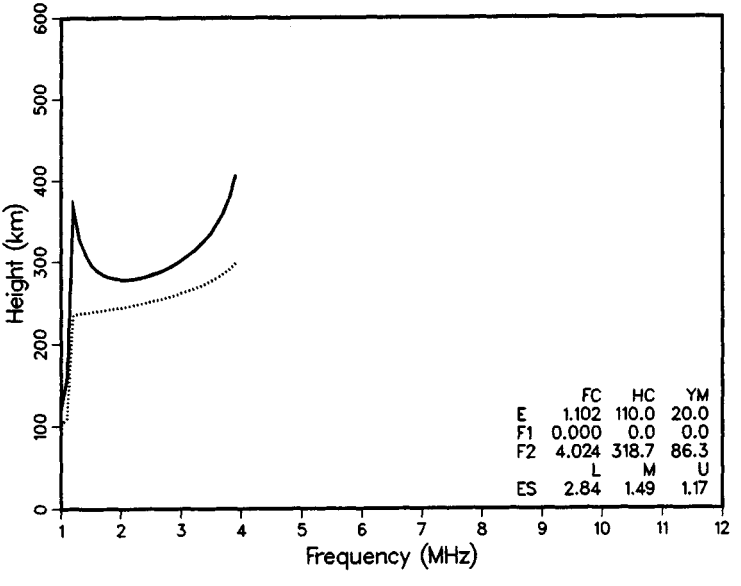

(b)

FIG. 24.9 The virtual (solid line) and true (dotted line) reflection heights are given for July, SSN = 50, and a mid-Atlantic-coast radar refraction area. (*a*) 1800 UTC is a daytime example, first hop. (*b*) 0800 UTC is a nighttime example.

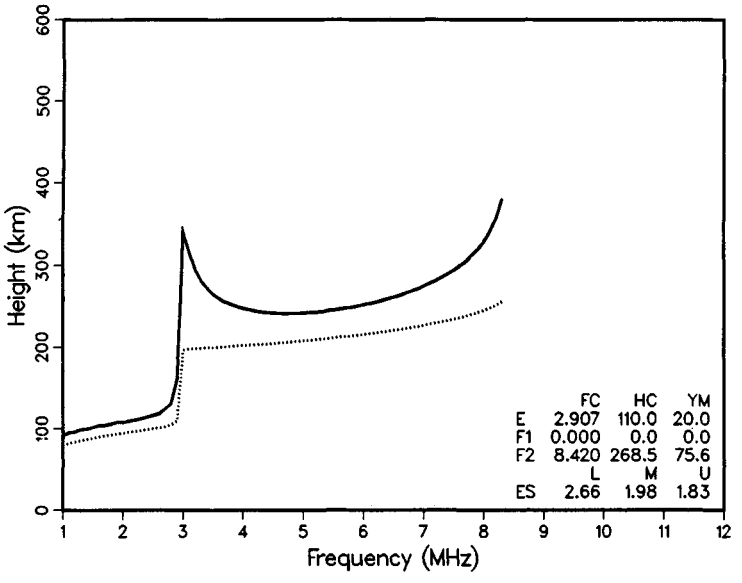

(a)

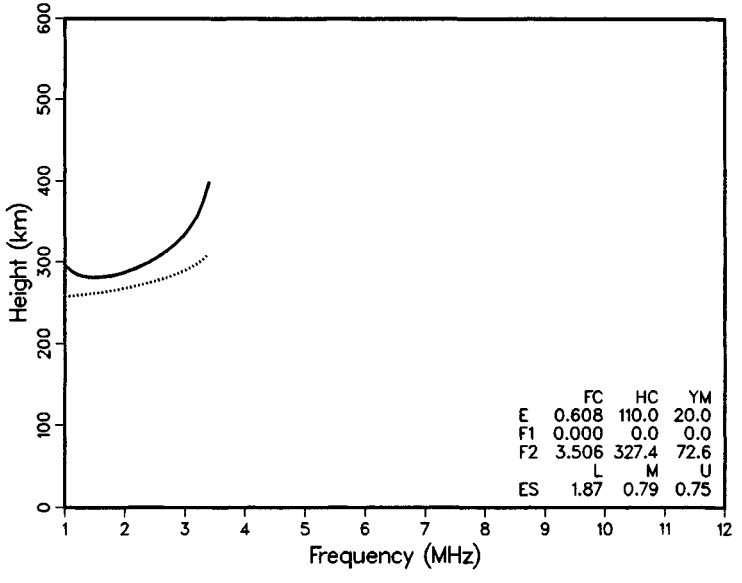

(b)

FIG. 24.10 Predicted ionograms as in Fig. 24.9, but in January. (*a*) 1800 UTC for day. (*b*) 0800 UTC for night.

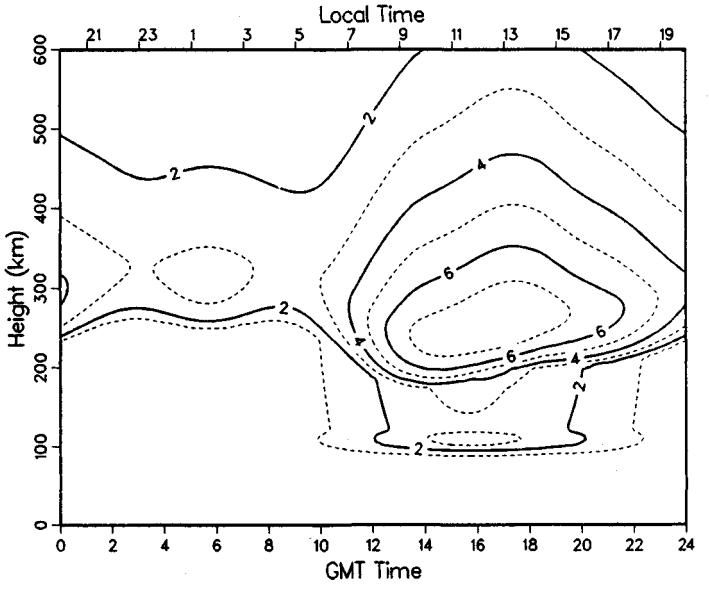

FIG. 24.11 Plasma- (critical-) frequency contours are given as a function of time of day for July; SSN = 50, latitude = 37.55°N, and longitude = 60.56°W.

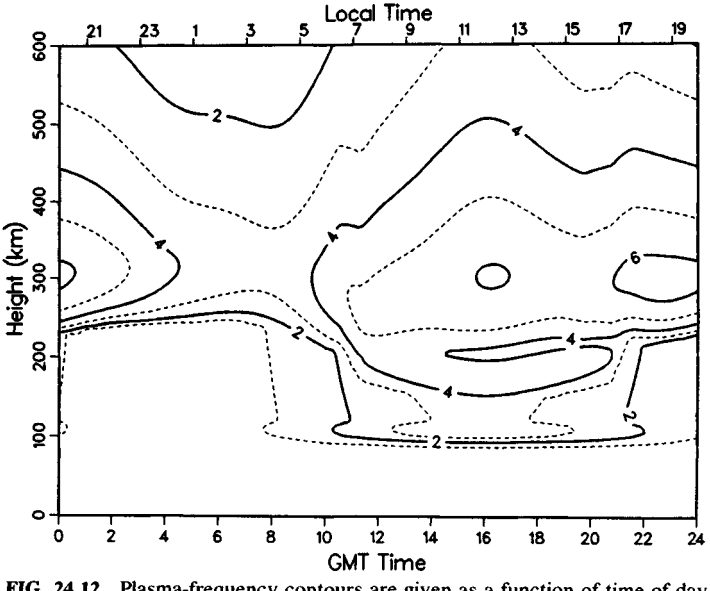

FIG. 24.12 Plasma-frequency contours are given as a function of time of day for January. Other controls are as in Fig. 24.11.

24.10 SKY-WAVE RADAR PERFORMANCE

The performance index used in this section will be the signal-to-noise ratio (*SNR*) indicated when using the transmission-medium model treated in Sec. 24.9 and the CCIR Report 322 noise discussed in Sec. 24.7. An additional need is a method to determine path effects. The detail with which path tracing is treated can vary greatly. A geometrical optics code that envolves integration along the ray as described by Jones and Stephenson[51] can provide paths in three dimensions, including delays and losses for both ordinary and extraordinary rays. When the details of electron distributions are uncertain, such comprehensive calculations are excessive. A number of other methods of path determination are available: for example, a path approximation technique goes with each of the ionospheric models mentioned in Sec. 24.9. For the performance exhibits treated here, the NRL-ITS Radar Performance Model will be used. This has been called RADAR C not quite correctly, but it is a lineal descendant of RADAR C.

NRL Memorandum Report 2500[52] describes the basic technique that will be used for path determinations. A simple closed-form virtual path trace, Snell's law for a spherically symmetric medium, is sequenced through elevation radiation angles in 1° increments. This process is incremented in 1-MHz steps over the radar's operating band. A vertical sounding of the ionosphere 700 km downrange has been used as the electron distribution for all one-hop paths, and a sounding 1400 km downrange is used for two-hop paths. Figures 24.9 and 24.10 gave a night and day example of the ionosphere 700 km downrange from a radar located at 38.65°N and 76.50°W looking east. Figure 24.13 gives constant plasma-frequency contours versus range from the radar for 0800 UTC, SSN 50, January

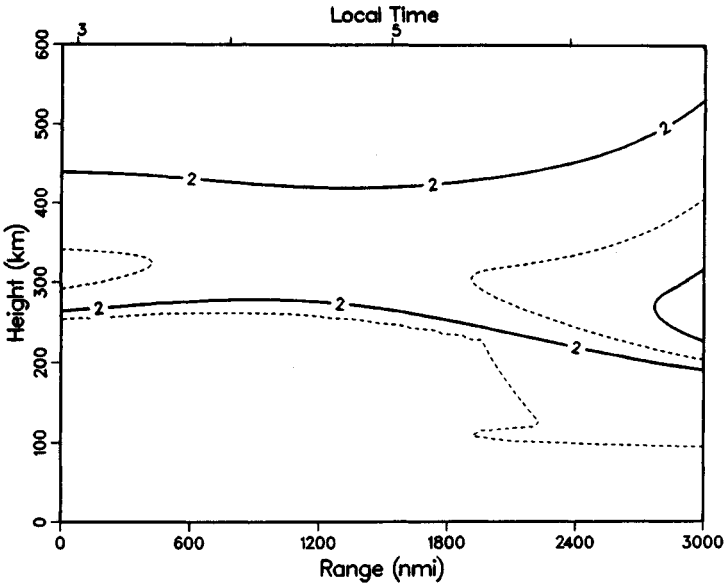

FIG. 24.13 Plasma-frequency contours are given, extending from the radar to a point east 3000 nmi downrange; January night example.

(night); and Fig. 24.14 for 1800 UTC (day). For the night case, the concentric spherical assumption from the 700-km downrange position will give paths that are slightly long for one-hop ranges. In the two-hop ranges the no-gradient assumption causes more distortion. In general, errors of this nature have little impact on performance prediction. However, near-real-time analysis for virtual range and azimuth correction to great-circle distance and bearing (grid registration) requires that tilt or gradient effects be taken into account. The daytime example has little horizontal gradient, and the simplifying assumption makes little difference. When better accuracy is desired, the correct vertical profile can be used for each radiation angle; also, gradients can be simulated by making the ionosphere nonconcentric with the earth. Both of these measures or something more complete should be used in radar performance assessment and management.

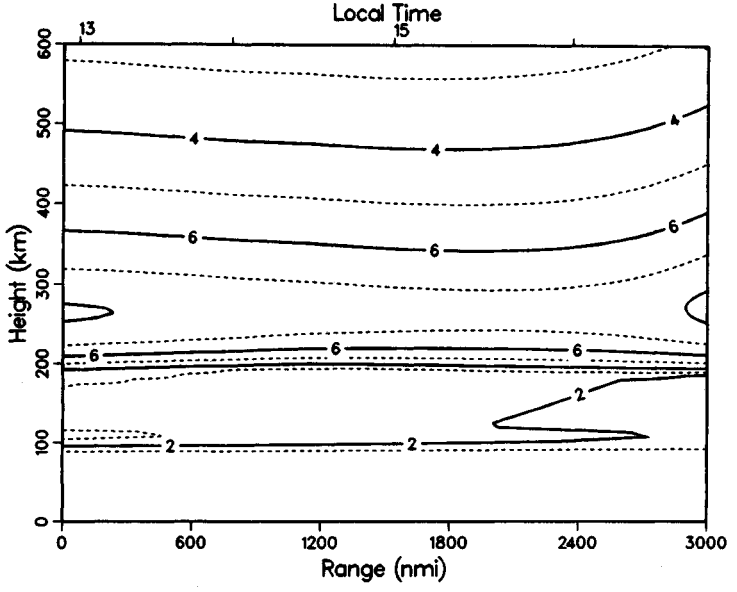

FIG. 24.14 Plasma-frequency contours are given, extending from the radar to a point east 3000 nmi downrange; January day example.

Figure 24.15 shows a performance prediction in the form of an oblique sounding. A typical sky-wave radar will be equipped with a vertical sounder and an oblique backscatter sounder for transmission-path analysis and to aid in radar-frequency management. Of course, the radar itself is an oblique sounder, but its sounding data is restricted to the frequency, waveform, and scan program of its primary surveillance task. An adjunct oblique sounder can present information in the form of Fig. 24.15 on earth backscatter echoes. In this prediction, *SNR* in decibels is plotted as a function of operating frequency and great-circle time delay or ground range. The numbers just above the abscissa (at 1-ms delay) are the noise powers in decibels below 1 W/Hz. For this plot the UTC time is 1800, SSN = 50, P_t = 200 kW, G_tG_r = 50 dB, T = 1 s, and σ = 20 dBsm. Figure 24.16 gives the corresponding night plot. The shape of these displays is quite similar to what would be seen with a diagnostic oblique sounding; the levels would gener-

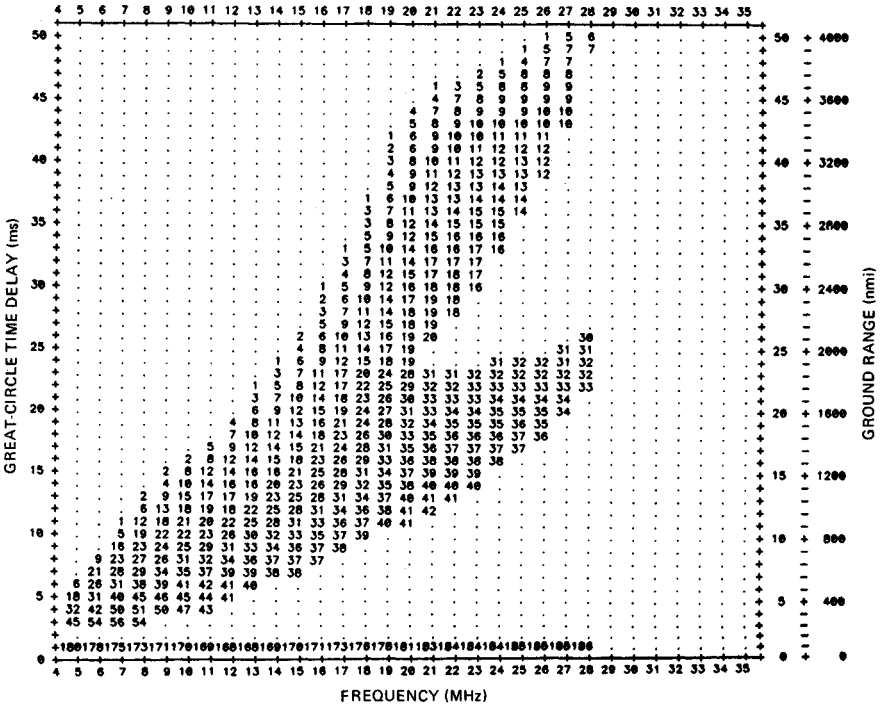

FIG. 24.15 *SNR* is given as a function of frequency and range in the form of a typical oblique backscatter sounding; January, 1800 GMT (day), SSN 50, location 38.65°N and 76.53°W, bearing 90°.

ally be greater since the resolution cell area times the surface scattering coefficient is generally much larger than 20 dBsm. Some of the night-day contrasts, such as available frequencies and difference in noise level for the same range, are evident. Also note that at night the 5-MHz lower frequency limit does not provide coverage closer than about 500 nmi. It should be remembered that this is a median SSN 50 calculation, and if consistent performance for ranges as close as 500 nmi is required during nights, a lower frequency limit should be selected to deal with periods of lower solar activity and the critical frequency distribution. The plots show that operation on a single frequency provides less than ±3 dB variation over a 500-nmi range interval. Also, if frequency selection had been made with a 2-MHz granularity instead of the 1 MHz used, the *SNR* would be reduced by only a decibel or so.

The performance-estimating aids that follow come from analyses as described above. After calculations as for oblique sounding, a range-ordered table of parameters is made. Parameter selections are made on the basis of the best *SNR* in each nominal 50-nmi interval, but the selection is adjusted to come from the adjacent lower frequency to avoid an optimistic bias. Then parameter plots are made as a function of range. The variables shown are losses, frequency, noise, and elevation radiation angle. The choice of range as the independent variable may seem artificial, but it is a useful approach for performance examination. With these curves the impact on radar *SNR* performance can be estimated for

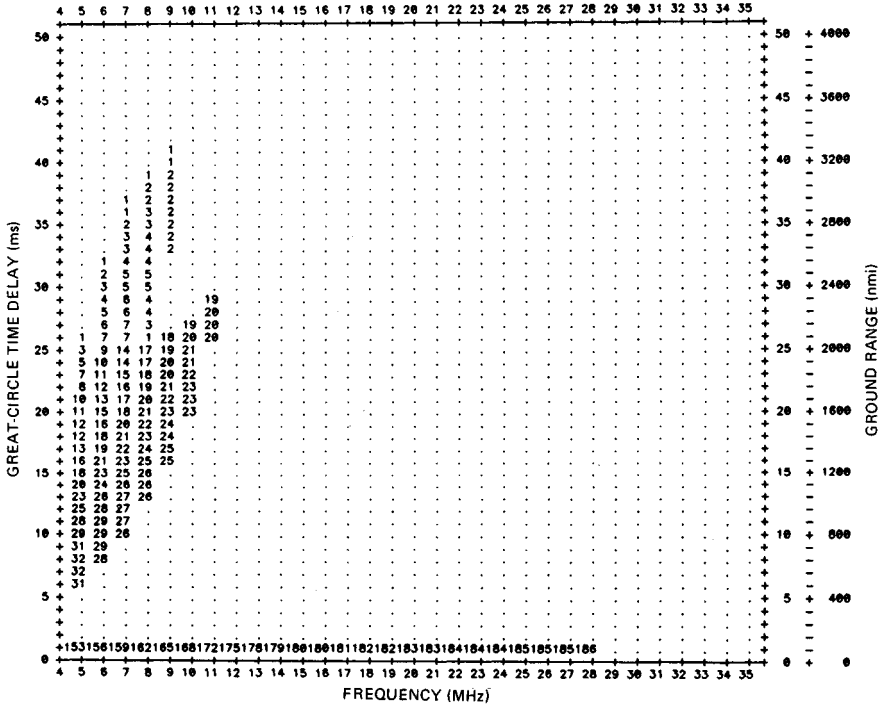

FIG. 24.16 *SNR* is given as a function of frequency and range in the form of an oblique sounding, as in Fig. 24.15, but for 0800 GMT (night).

selected antenna gain patterns, transmitted powers, target RCS, and coherent integration times (CIT). Figure 24.17 is an example for January with low solar activity in daytime. The R^4 loss is the fourth power of range to the target in meters given in decibels. $R^4 + L$ adds nondeviative absorption, deviative absorption, sporadic-E obscuration, and ground-reflection losses if there is more than one hop. The sharp increase in loss just before 2000 nmi is caused by transition from one to two hops; for two hops the lossy D region is transited twice as many times, ground-reflection loss is added, and required operation at a lower frequency increases loss. The jagged curve in the transition region is due to the parameter selection process; in radar operation the frequency would be selected to minimize transition effects. The frequency, radiation angle, and noise power per hertz that go with this site and look direction are also plotted. An example will be treated. It will be convenient to write the radar equation (24.1) in decibels:

$$SNR = P_{av} + G_t + G_r + \lambda^2 + T + \text{RCS} + F_p - (4\pi)^3 - (R^4 + L) - N$$

Select 1000 nmi as the range. Then the frequency is 17.5 MHz (wavelength = 17.1 m and $\lambda^2 = 25$ dB), noise power = -175 dB, and $R^4 + L = 261$ dB. Choose 53 dBW for P_{av}, 20 dB for G_t, 30 dB for G_r, 0 dBs for T, 20 dBsm for RCS, and 6 dB for F_p.

$$SNR = 53 + 20 + 30 + 25 + 0 + 20 + 6 - 33 - 261 - (-175) = 35 \text{ dB}.$$

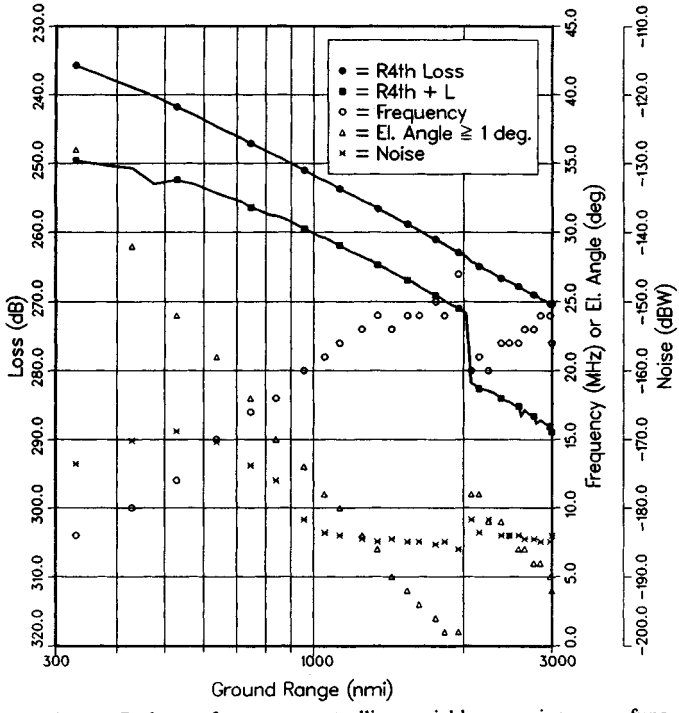

FIG. 24.17 Radar performance-controlling variables are given as a function of range; January, 1800 UTC, SSN 50.

Figure 24.18 shows the performance indicated with these assumptions for all ranges. A path factor enhancement of 6 dB has been chosen as an estimate of constructive multipath interference for an aircraft target that is effective in target detection. The beamwidth has been taken to be 5.7° and the surface scattering coefficient to be −35 dB, and with a 12 dB path enhancement the clutter level has been plotted. The clutter-to-noise ratio (*CNR*) at 1000 nmi is about 82 dB. For the constant beamwidth assumed, the clutter-to-signal ratio increases with range and is 47 dB at 1000 nmi. Large clutter-to-signal ratios are typical of HF radar; some form of doppler filtering is used to separate targets from clutter.

In Figs. 24.19 through 24.26 the performance-estimating curves are given for four seasons, night and day, and high and low solar activity. The permissible frequency selection is set between 5 and 28 MHz, and antenna radiation is not considered below an elevation angle of 1°. The analyses were made for a radar off the mid-Atlantic coast of the United States and should be a good approximation for any location where transmission paths are through the middle magnetic latitudes. This OTH performance presentation can be used to decide on the antenna patterns and powers required for specific targets and missions, or it can be used to exhibit periods of enhanced or degraded performance for an existing design. In looking at the performance index curves with radar range as the independent variable,

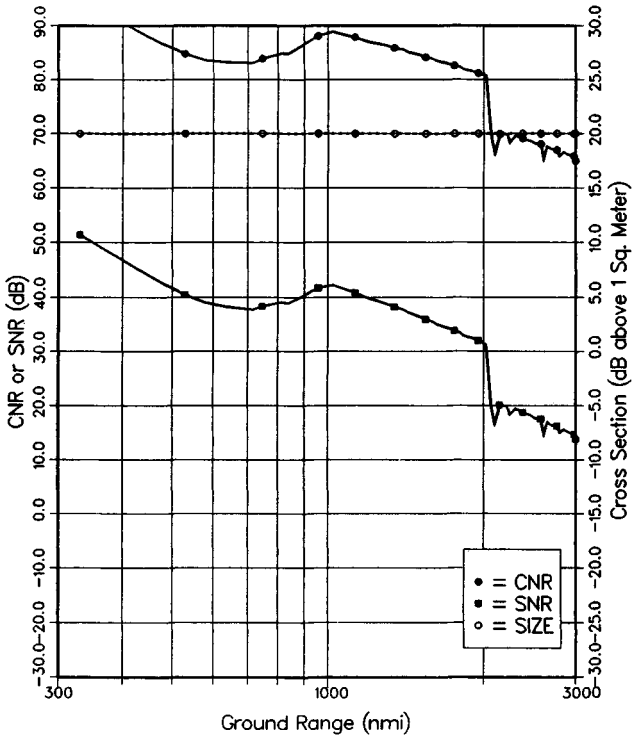

FIG. 24.18 A specific example of *SNR* and clutter-to-noise ratio (*CNR*) is determined by using Fig. 24.17. The target RCS is labeled "size" and is considered constant.

1. Summer shows much greater losses than other seasons.
2. Except for summer, night losses are only slightly less than day losses.
3. Night noise is much greater than day noise.
4. For a specific range, optimum frequencies vary by 3:1.

Several qualifiers should be kept in mind. At other geographic locations, the appropriate CCIR noise should be selected or, better yet, measured noise used. For radars that use auroral zone paths, specific analyses are required and target obscuration by spread-in-doppler clutter must be considered. The performance estimates from the figures assume that the radar design and waveforms are such that external noise is the control. The use of a single description for night and day gives a fair representation, but the transition from night to day is very abrupt and requires careful frequency management in radar operation. The ionospheric description that has been used is for what has been termed the *quiet ionosphere*; there will be a few hours per year when performance is very inferior to that predicted.

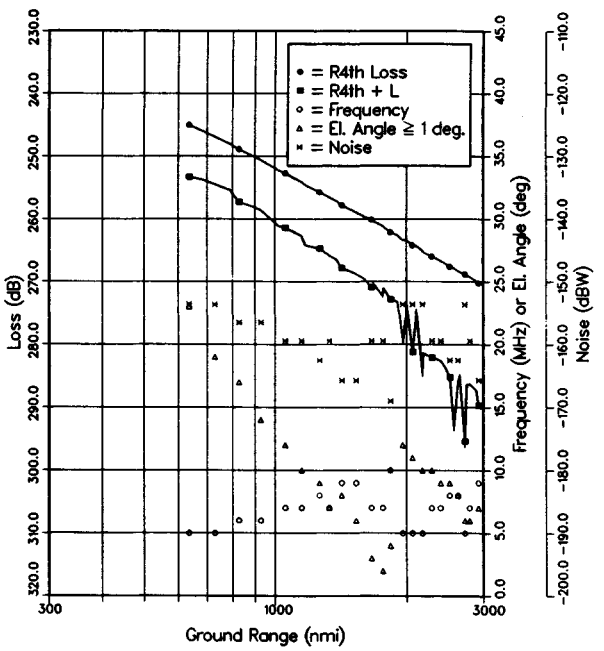

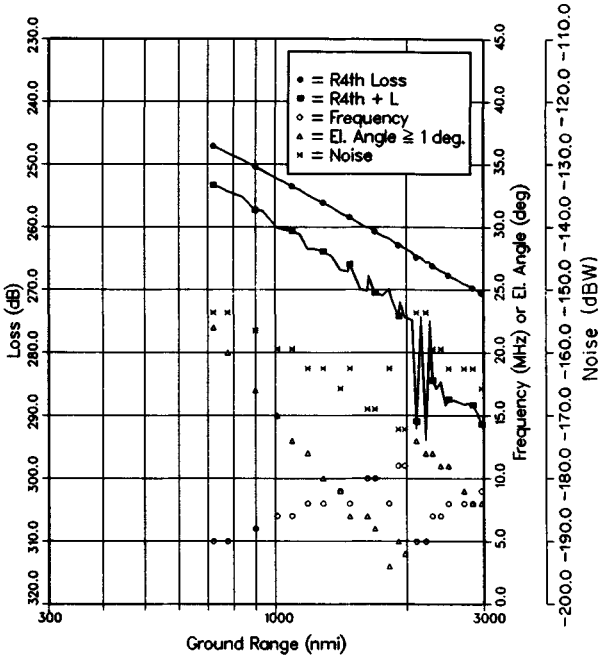

FIG. 24.19 Radar performance estimate; January, 0800 UTC. (*a*) SSN = 10. (*b*) SSN = 100.

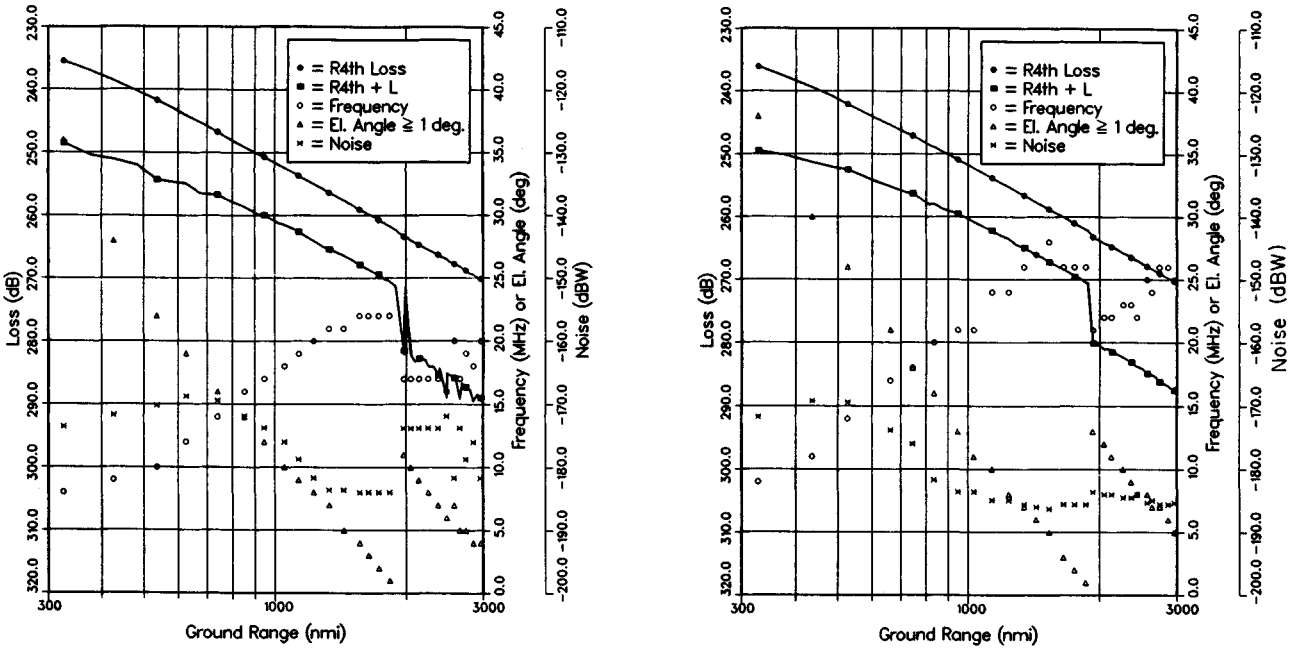

FIG. 24.20 Radar performance estimate; January, 1800 UTC. (*a*) SSN = 10. (*b*) SSN = 100.

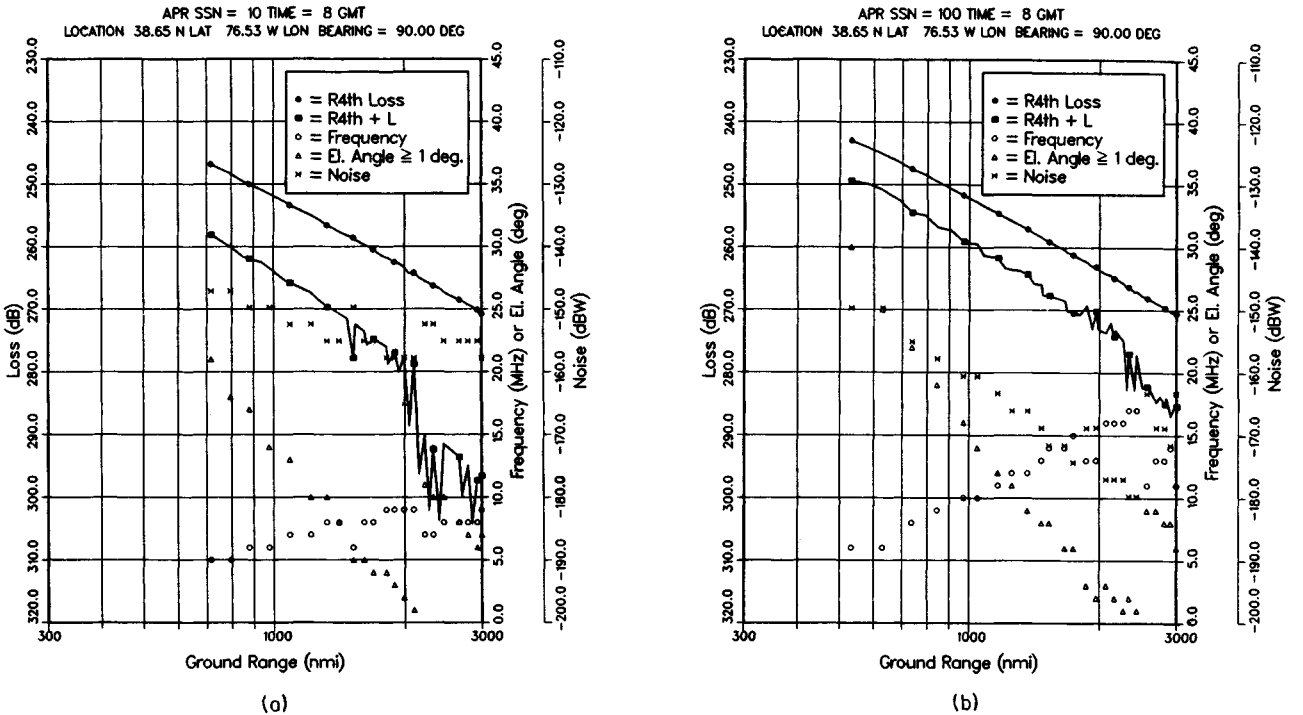

FIG. 24.21 Radar performance estimate; April, 0800 UTC. (*a*) SSN = 10. (*b*) SSN = 100.

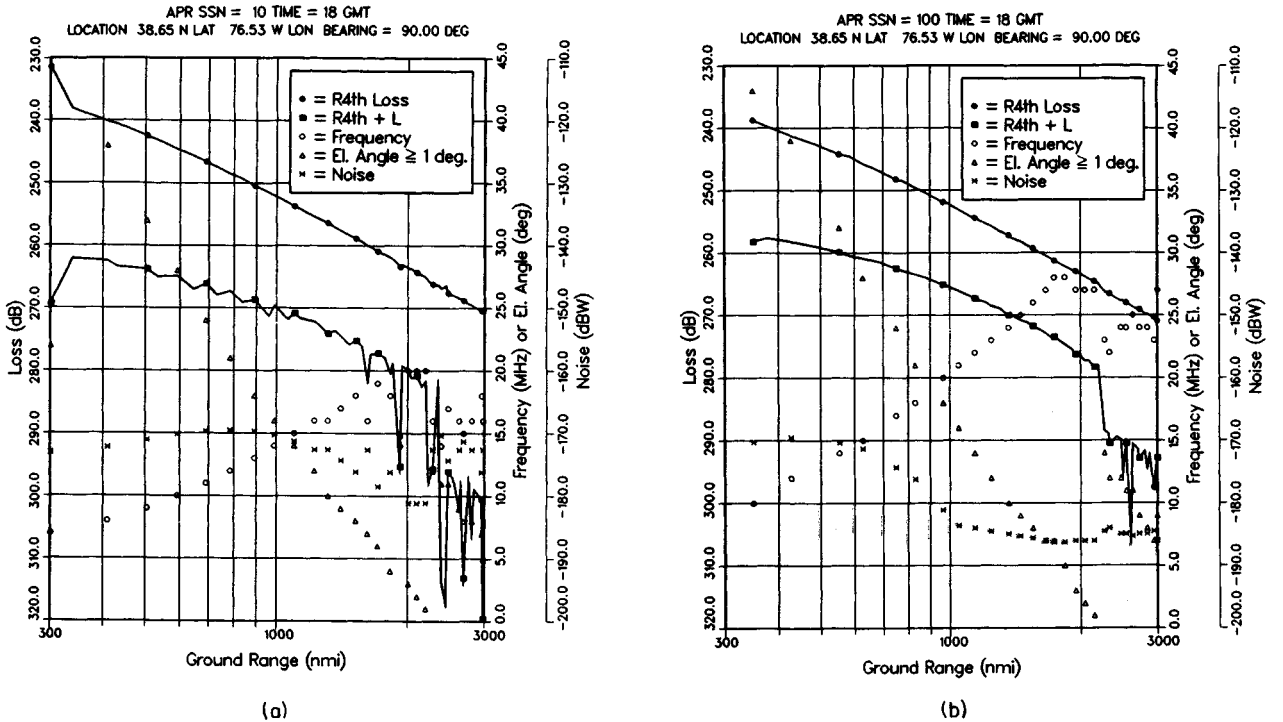

FIG. 24.22 Radar performance estimate; April, 1800 UTC. (*a*) SSN = 10. (*b*) SSN = 100.

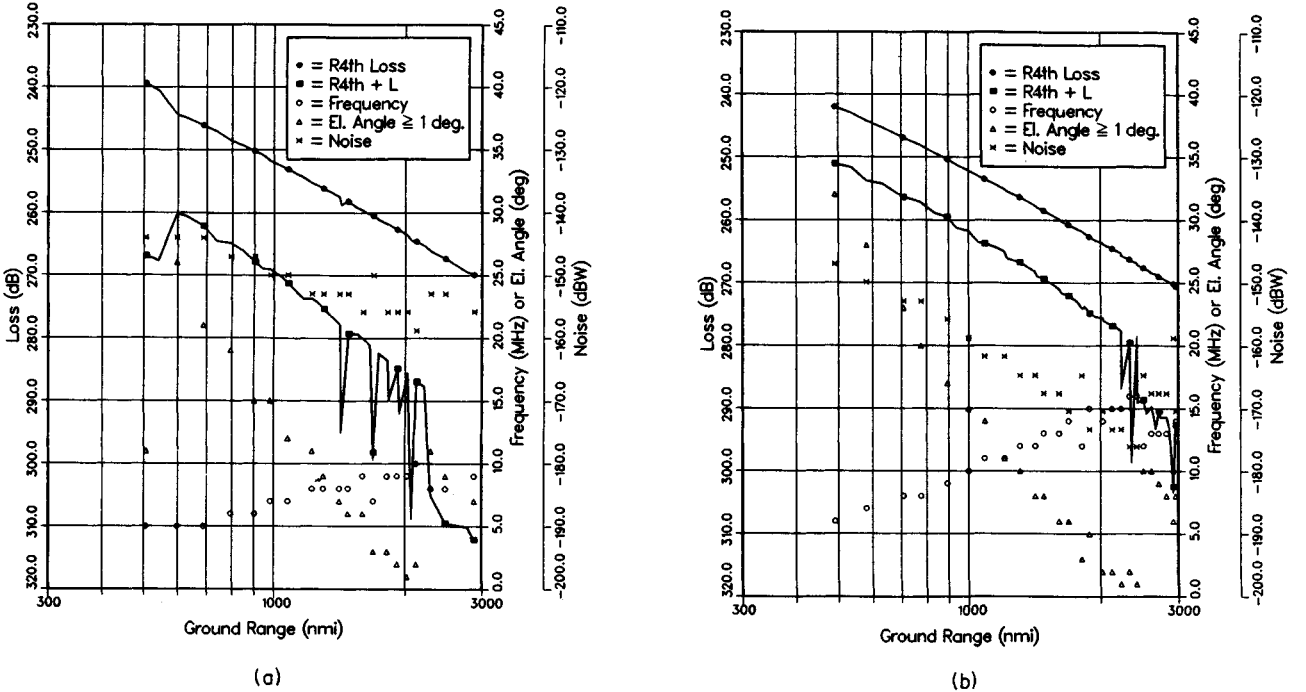

FIG. 24.23 Radar performance estimate; July, 0800 UTC. (*a*) SSN = 10. (*b*) SSN = 100.

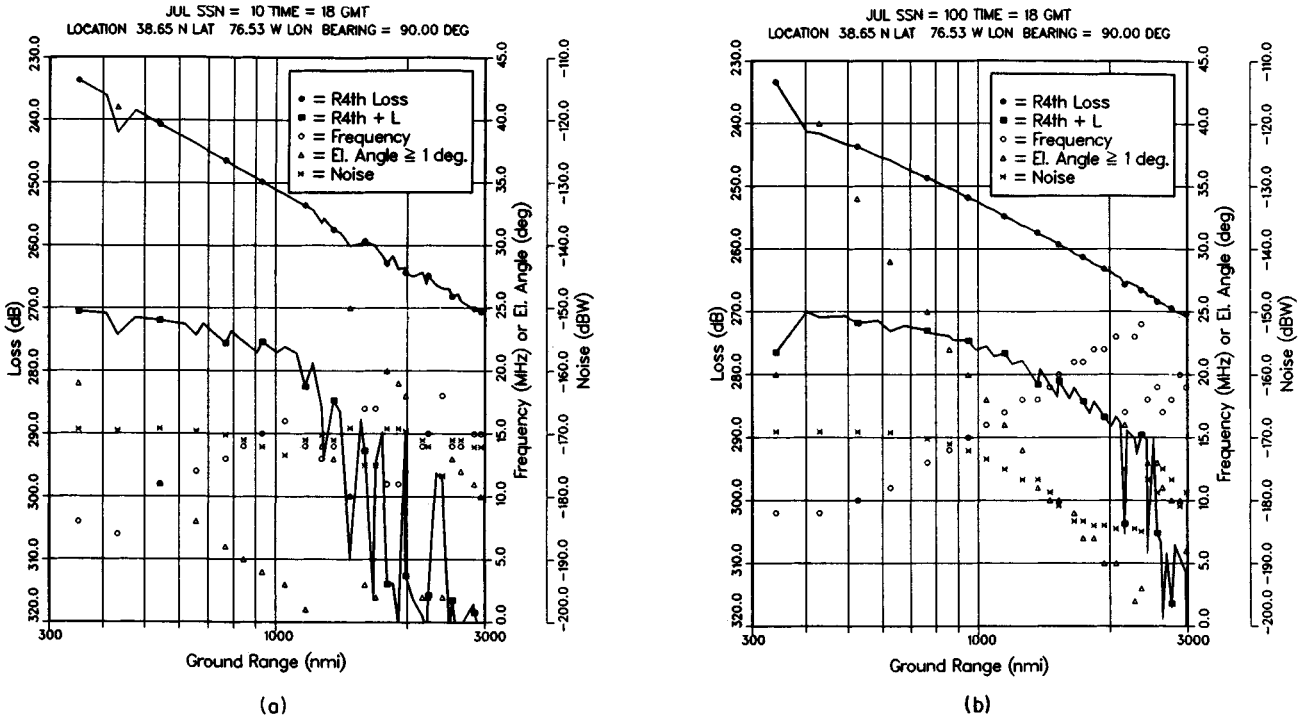

FIG. 24.24 Radar performance estimate; July, 1800 UTC. (*a*) SSN = 10. (*b*) SSN = 100.

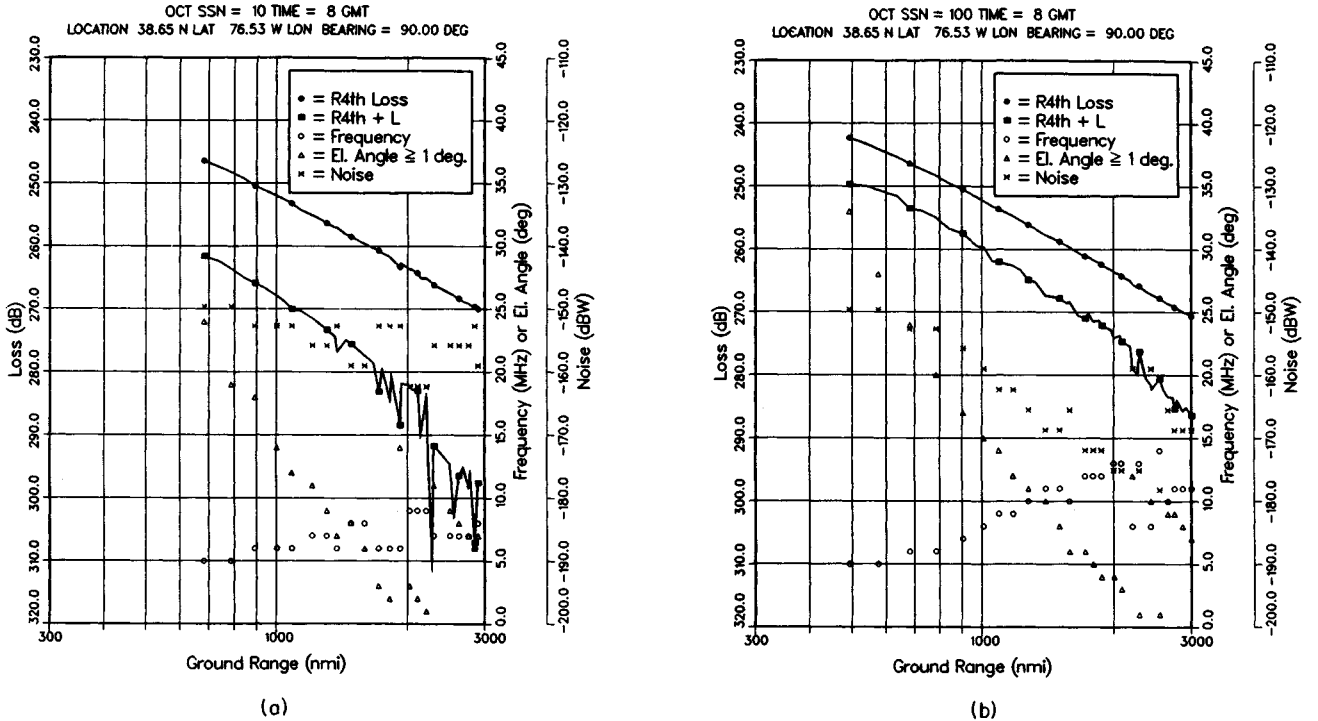

FIG. 24.25 Radar performance estimate; October, 0800 UTC. (*a*) SSN = 10. (*b*) SSN = 100.

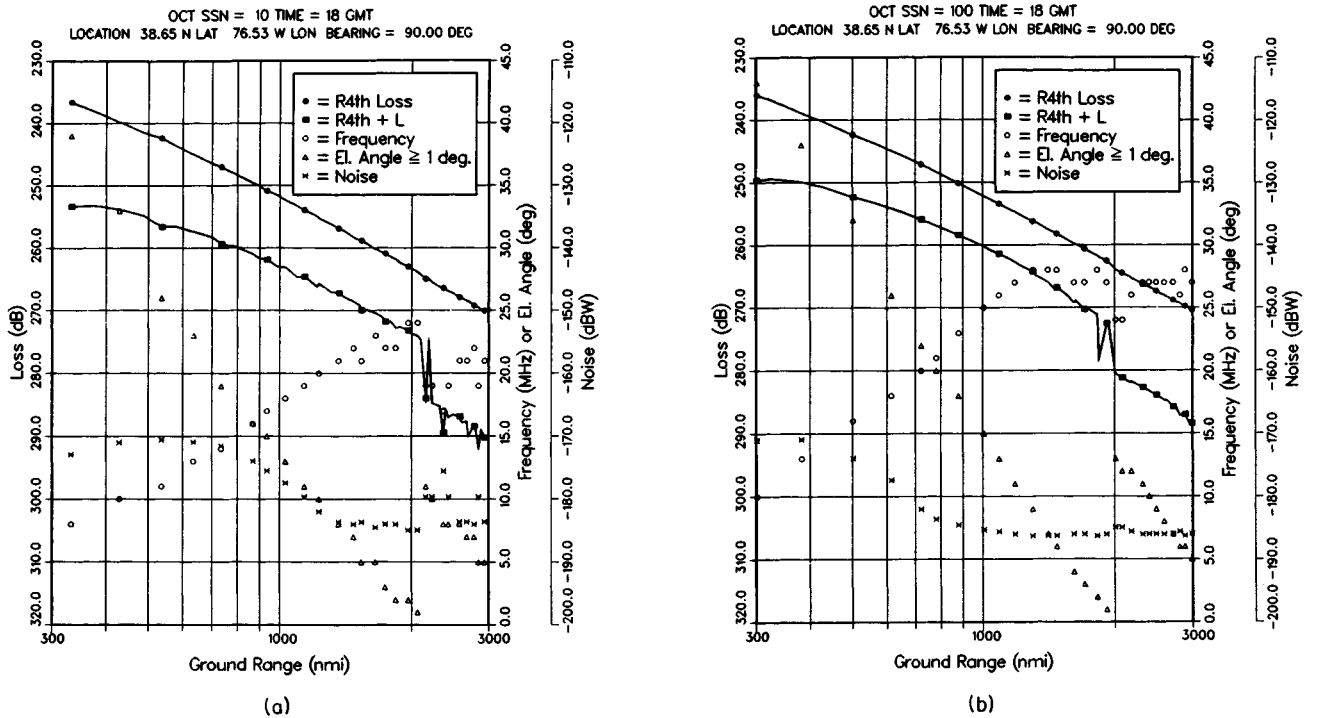

FIG. 24.26 Radar performance estimate; October, 1800 UTC. (*a*) SSN = 10. (*b*) SSN = 100.

24.11 RECEIVER-PROCESSOR

The prediction method indicated above is based upon long-term medians of vertical soundings, measured path losses, and observed noise. The statistical distributions are for a particular hour over days of the month or season. These kinds of statistics are insufficient to define the requirements for detection and tracking. An example will be given on the basis of a long dwell on a target using a constant frequency. The data will be used to indicate the required dynamic range and processor size and to show the input of the detection and tracking process. The amplitude levels in Fig. 24.27 are given in decibels relative to an arbitrary reference. Figure 24.27*a* gives a short time history of received power amplitude versus doppler frequency in one range gate. The waveform repetition frequency (wrf) was 20 Hz. Noise (*N*) samples were taken at wrf/2, target samples (*T*) on a target peak, and approach (*A*) and recede (*R*) on the resonant ocean wave peaks; *N*, *T*, *A*, and *R* are plotted in Fig. 24.27*b*. For this processing with a CIT of 12.8 s, the doppler filter bandwidth is a nominal 0.08 Hz, and at least 256 doppler filters should be used. The distance between the minimum noise points and the maximum clutter points is of the order of 100 dB, which indicates the dynamic range requirement if small targets are to be seen. For digital processing, an analog-to-digital (A/D) converter of at least 16-bit accuracy is in order. If data is processed

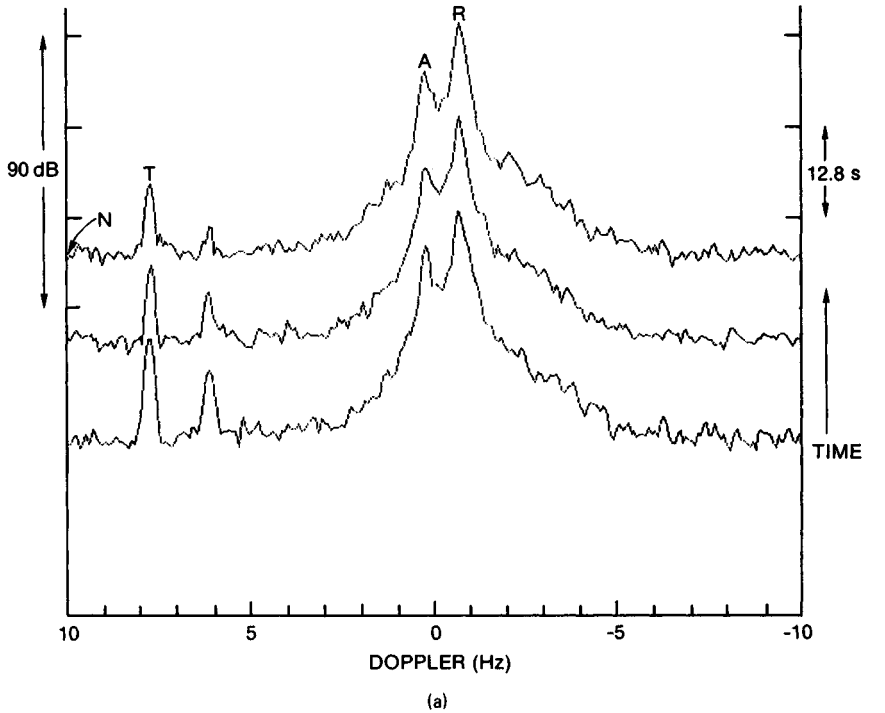

FIG. 24.27 (*a*) Amplitude versus doppler is plotted for a sequence of three 12.8-s coherent dwells. Indicated are a target marked *T*, the approach and recede resonant sea clutter peaks marked *A* and *R*, and the position for taking the noise sample marked *N*.

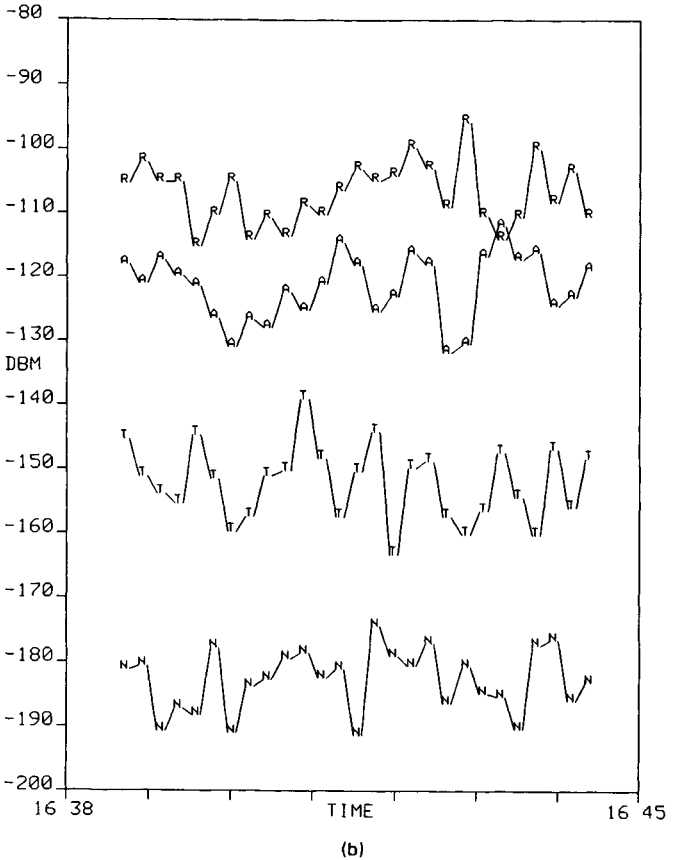

(b)

FIG. 24.27 *(Continued) (b)* Target, clutter peaks, and noise are plotted versus time for a longer sequence of data as in *a*.

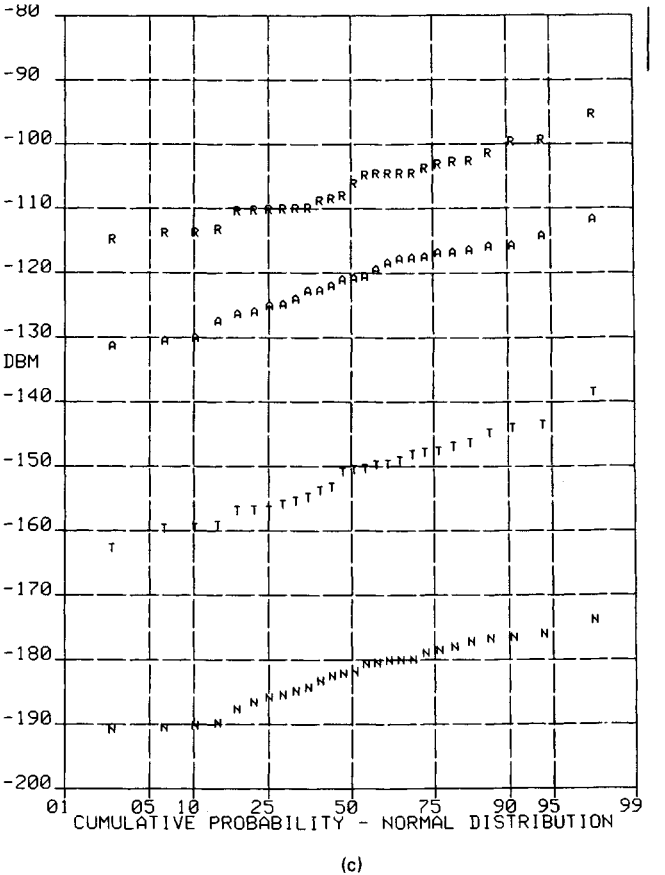

(c)

FIG. 24.27 *(Continued) (c)* Amplitude distributions of target, clutter peaks, and noise are plotted.

for a radar operating as shown in Fig. 24.1, there will be a 500-nmi range extent at a 10-kHz resolution bandwidth requiring about 60 range gates; I and Q processing to expose unambiguously target dopplers between $\pm$wrf/2 requires a sample rate of 40 kHz. For the Fig. 24.1 example, 16 simultaneous receiver-processor channels are required for the multiple receive beams. Figure 24.27*c* gives the corresponding power-level distributions. These approximately log-normal distributions are typical. The wide-area surveillance application makes automatic detection and tracking very desirable; the single transmitter footprint shown in Fig.24.1 has 800 receive range-azimuth cells. Tracker requirements differ from those of other sensors in that it is generally necessary to have thresholds that permit many natural responses. It is common practice to defer target declaration until a track is recognized and thereby to reduce the false-alarm rate.

24.12 GROUND-WAVE RADAR PERFORMANCE

Ground-wave propagation as defined here will include all but sky-wave paths. That is, the paths or illumination considered are direct line-of-sight and by sea-

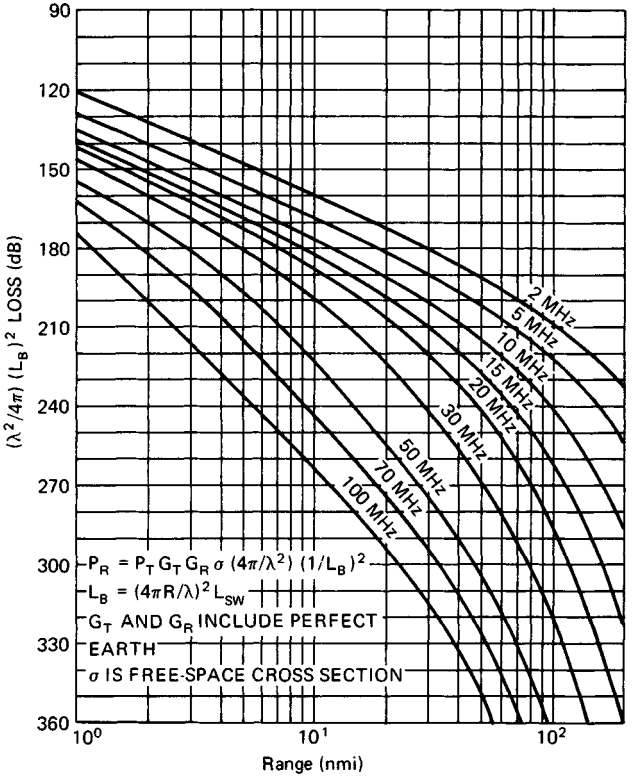

FIG. 24.28 Curves for estimating ground-wave radar performance are given as a function of range and are parametric in frequency. The surface is considered smooth, target and antenna heights are 2 m, conductivity is assumed to be 5 S/m, and the dielectric constant is 80.

surface reflection when radar and target are above the horizon and illumination in the penumbra and shadow region by a surface-attached wave. The feature that causes this propagation to be considered is that vertical polarization provides useful illumination down to the sea surface beyond the optical horizon. Figure 24.28 gives an example of ground-wave radar performance, parametric in frequency for the case in which both the radar antenna and the target are near the sea surface. These curves are for a smooth surface and use a ⅓ earth radius to approximate atmospheric refraction effects. The propagation code is due to Berry

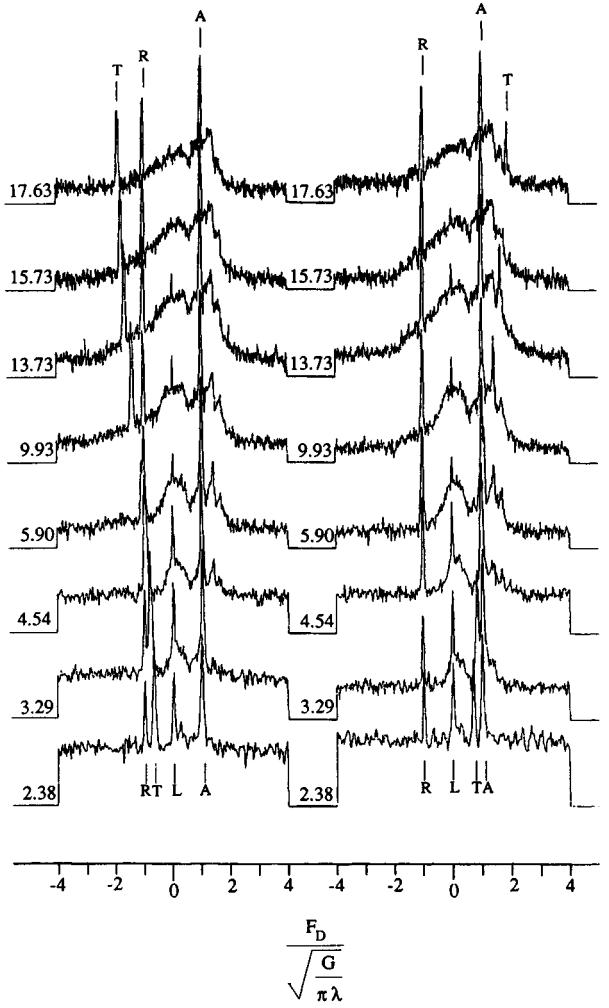

FIG. 24.29 Examples of a target *T* are shown when approaching (right) and receding (left) in the presence of the sea echo. The format is of received power versus normalized doppler for seven radar operating frequencies. The resonant wave or Bragg peaks are marked *A* for approaching and *R* for receding. The peak at zero frequency is due to a stationary target in an antenna sidelobe.

and Chrisman,[53] and it is quite flexible, permitting antenna and target altitudes, surface conductivity and permittivity, polarization, and frequency to be specified. Sea roughness can be taken into account by using the work of Barrick.[54] Path-loss descriptors such as shown in Fig. 24.28 can be used to estimate performance. For example, consider a radar at 5 MHz with an average power of 10 kW (40 dBW), a transmit-receive antenna gain product of 15 dB, and a target at 100 nmi with an RCS of 20 dBsm; then the received power

$$P_r = 40 + 15 + 20 - 222 = -147 \text{ dBW}$$

By using the January nighttime noise as given in Fig. 24.6*b*,

$$SNR = P_r - N = -147 + 153 = 6 \text{ dB}$$

And if 10-s coherent processing time is used,

$$SNR = 16 \text{ dB}$$

Figure 24.29 provides a display of a 13-kn target and the sea echo as seen by a ground-wave radar. This is a family of received power versus doppler frequency plots over seven operating frequencies and for a target both approaching and receding. The abscissa units are in doppler normalized to the resonant wave or Bragg frequency; therefore, the resonant wave responses peak at ± 1. The amplitude range for each plot is 60 dB. The peaks at zero-doppler frequency are due to land in an antenna sidelobe. The target doppler coincides with a resonant line at 4.93 Mhz; it is between the lines below that frequency and outside them for frequencies above. The approach resonant wave peak is about 20 dB larger than the recede peak, indicating an almost direct sea into the radar. The processing used in developing these displays was 200-s CIT and 30-min averaging. This order of time for processing is appropriate for surface-target speeds and ground-wave radar; it also shows in doppler detail the form of the sea echo.

REFERENCES

1. Headrick, J. M., and M. I. Skolnik: Over-the-Horizon Radar in the HF Band, *Proc. IEEE*, vol. 62, pp. 664–673, June 1974.
2. Barnum, J. R.: Ship Detection with High Resolution HF Skywave Radar, *IEEE J. Ocean. Eng.*, vol. OE-11, pp. 196–210, April 1986.
3. Boutacoff, D. A.: Backscatter Radar Extends Early Warning Times, *Def. Electron.*, vol. 17, pp. 71–83, May 1985.
4. Sinnott, D. H.: The Jindalee Over-the-Horizon Radar System, *Conf. Air Power in the Defence of Australia*, Australian National University, Research School of Pacific Studies, Strategic and Defence Studies Centre, Canberra, July 14–18, 1986.
5. Wylder, J.: The Frontier for Sensor Technology, *Signal*, vol. 41, pp. 73–76, March 1987.
6. Guest editorial and invited papers in special issue on high-frequency radar for ocean and ice mapping and ship location: *IEEE J. Ocean. Eng.*, vol. OE-11, April 1986.

7. Kolosov, A. A. (ed.): "Fundamentals of Over-the-Horizon Radar," in Russian, *Radio i svyaz*, 1984. Also a translation by W. F. Barton, Artech House, Norwood, Mass., 1987.
8. Greenwald, R. A., K. B. Baker, R. A. Hutchins, and C. Hanuise: An HF Phased Array Radar for Studying Small-Scale Structure in the High Latitude Ionosphere, *Radio Sci.*, vol. 20, pp. 63–79, January–February 1985.
9. ITT Avionics Division, Electro-Physics Laboratories: EPL Model ATL-75 Transmitter for Radar and Communication, *IR&D Project Rept.* 274, *Results of Performance Measurements*, January 1975.
10. Hoft, D. J., and Fuat Agi: Solid State Transmitters for Modern Radar Applications, *CIE Int. Radar Conf. Rec.*, pp. 775–781, Nov. 4–7, 1986.
11. Guest editorial and invited papers in special issue on shortwave broadcasting, *IEEE Trans. Broadcast.*, vol. 34, June 1988.
12. Sweeney, L. E.: Spatial Properties of Ionospheric Radio Propagation as Determined with Half-Degree Azimuthal Resolution, *Stanford Electron. Lab. Tech. Rept.* 155 *SU-SEL*-70-034, Stanford University, June 1970.
13. Lynch, J. T.: Aperture Synthesis for HF Radio Signals Propagated via the F-Layer of the Ionosphere, *Stanford Electron. Lab. Tech. Rept.* 161 *SU-SEL*-70-066, Stanford University, September 1970.
14. Johnson, R. C., and H. Jasik (eds.): "Antenna Engineering Handbook," 2d ed., McGraw-Hill Book Company, New York, 1984.
15. Kurashov, A. G. (ed.): "Shortwave Antennas," 2d ed., in Russian, *Radio i svyaz*, January 1985.
16. Rice, S. O.: Reflection of Electromagnetic Waves from Slightly Rough Surfaces, in Kline, M. (ed.): "Theory of Electromagnetic Waves," Interscience Publishers, New York, 1951, pp. 351–378.
17. Pierson, W. J., G. Neumann, and R. W. James: Practical Methods for Observing and Forecasting Ocean Waves by Means of Wave Spectra and Statistics, *H.O. Pub.* 603, chap. 1, Hydrographic Office, U.S. Navy, 1960.
18. Crombie, D. D.: Doppler Spectrum of the Sea Echo at 13.56 Mcs, *Nature*, vol. 175, pp. 681–682, 1955.
19. Barrick, D. E.: First Order Theory and Analysis of MF/HF/VHF Scatter from the Sea, *IEEE Trans.*, vol. AP-20, pp. 2–10, January 1972.
20. Pierson, W. J., and L. Moskowitz: A Proposed Spectral Form for Fully Developed Wind Seas Based on the Similarity Theory of S. A. Kitaigordskii, *J. Geophys. Res.*, vol. 69, no. 24, pp. 5181–5190, 1964.
21. Barrick, D. E., J. M. Headrick, R. W. Bogle, and D. D. Crombie: Sea Backscatter at HF: Interpretation and Utilization of the Echo, *Proc. IEEE*, vol. 62, pp. 673–680, June 1974.
22. Clancy, R. M., J. E. Kaitala, and L. F. Zambresky: The Fleet Numerical Oceanography Center Global Spectral Ocean Wave Model, *Bull. Am. Meteorol. Soc.*, vol. 67, no. 5, May 1986.
23. Long, A. E., and D. B. Trizna: Mapping of North Atlantic Winds by HF Radar Sea Backscatter Interpretation, *IEEE Trans.*, vol. AP-21, pp. 680–685, September 1973.
24. Ahearn, J. L., S. R. Curley, J. M. Headrick, and D. B. Trizna: Tests of Remote Skywave Measurment of Ocean Surface Conditions, *Proc. IEEE*, vol. 62, pp. 681–686, June 1974.
25. Anderson, S. J.: Remote Sensing with the Jindalee Skywave Radar, *IEEE J. Ocean. Eng.*, vol. OE-11, pp. 158–163, April 1986.
26. Trizna, D. B., J. C. Moore, J. M. Headrick, and R. W. Bogle: Directional Sea Spectrum Determination Using HF Doppler Radar Techniques, *IEEE Trans.*, vol. AP-25, pp. 4–11, January 1977.

27. Barrick, D. E.: Extraction of Wave Parameters from Measured HF Radar Sea-Echo Spectra, *Radio Sci.*, vol. 12, no. 3, p. 415, 1977.

28. Lipa, B.: Derivation of Directional Ocean-Wave Spectra by Integral Inversion of Second-Order Radar Echoes, *Radio Sci.*, vol. 12, no. 3, p. 425, 1977.

29. Trizna, D. B.: Estimation of the Sea Surface Radar Cross Section at HF from Second-Order Doppler Spectrum Characteristics, *Naval Res. Lab. Rept.* 8579, May 1982.

30. Pilon, R. O., and J. M. Headrick: Estimating the Scattering Coefficient of the Ocean Surface for High-Frequency Over-the-Horizon Radar, *Naval Res. Lab. Memo. Rept.* 5741, May 1986.

31. Trizna, D. B., and J. M. Headrick: Ionospheric Effects on HF Over-The-Horizon Radar, in Goodman, J. M. (ed.): *Proc. Effect Ionosphere on Radiowave Syst.*, ONR/AFGL-sponsored, pp. 262–272, Apr. 14–16, 1961.

32. Elkins, T. J.: A Model for High Frequency Radar Auroral Clutter, *RADC Rept. TR-80-122*, March 1980.

33. Burke, G. J., and A. J. Poggio: Numerical Electromagnetic Code (NEC)—Method of Moments, *NOSC Tech. Doc.* 116, 1981.

34. Walton, E. K., and J. D. Young: The Ohio State University Compact Radar Cross Section Measurement Range, *IEEE Trans.*, vol. AP-32, pp. 1218–1223, November 1984.

35. Bogle, R. W., and D. B. Trizna: Small Boat Radar Cross Sections, *Naval Res. Lab. Memo. Rept.* 3322, July 1976.

36. CCIR (International Radio Consultative Committee): World Distribution and Characteristics of Atmospheric Radio Noise, *CCIR Rept.* 322, International Telecommunications Union, 1964.

37. Spaulding, A. D., and J. S. Washburn: Atmospheric Radio Noise: Worldwide Levels and Other Characteristics, *NTIA Rept.* 85-173, National Telecommunications and Information Administration, April 1985.

38. Lucas, D. L., and J. D. Harper: A Numerical Representation of CCIR Report 322 High Frequency (3–30 Mcs) Atmospheric Radio Noise Data, *Nat. Bur. Stand. Note* 318, Aug. 5, 1965.

39. Ortenburger, L. N., D. A. Schaefer, F. W. Smith, and A. J. Kramer: Prediction of HF Noise Directivity from Thunderstorm Probabilities, *GTE Sylvania Rept. EDL-M1379*, 1971.

40. Lucas, D. L.: Predictions of Backscatter Clutter Power in the Radar C Computer Program, final report on NRL Contract N0014-84-C-2451; CU5-36903, University of Colorado, Boulder, June 9, 1986.

41. Davies, K.: "Ionospheric Radio Propagation," *Nat. Bur. Stand. Monog.* 80, Apr. 1, 1965.

42. Jursa, A. S. (ed.): "Handbook of Geophysics and the Space Environment," Air Force Geophysics Laboratory, AFSC, U.S. Air Force, 1985.

43. Lucas, D. L., and G. W. Haydon: Predicting Statistical Performance Indexes for High Frequency Telecommunications Systems, *ESSA Tech. Rept. IER* 1 *ITSA* 1, U.S. Department of Commerce, 1966.

44. Barghausen, A. L., J. W. Finney, L. L. Proctor, and L. D. Schultz: Predicting Long-Term Operational Parameters of High-Frequency Sky-Wave Communications Systems, *ESSA Tech. Rept. ERL* 110-*ITS* 78, U.S. Department of Commerce, 1969.

45. Headrick, J. M., J. F. Thomason, D. L. Lucas, S. McCammon, R. Hanson, and J. Lloyd: Virtual Path Tracing for HF Radar Including an Ionospheric Model, *Naval Res. Lab. Memo. Rept.* 2226, March 1971.

46. Teters, L. R., J. L. Lloyd, G. W. Haydon, and D. L. Lucas: Estimating the Performance of Telecommunication Systems Using the Ionospheric Transmission Channel—

Ionospheric Communications Analysis and Prediction Program Users Manual, *Nat. Telecom. Inf. Adm. NTIA Rept.* 83-127, July 1983.

47. Hatfield, V. E.: HF Communications Predictions 1978 (An Economical Up-to-Date Computer Code, AMBCOM), *Solar Terrestrial Preduction Proc.*, vol. 4, in Donnelley, R. F. (ed.): "Prediction of Terrestrial Effects of Solar Activity," National Oceanic and Atmospheric Administration, 1980.
48. Lucas, D. L.: Ionospheric Parameters Used in Predicting the Performance of High Frequency Skywave Circuits, Interim Report on NRL Contract N00014-87-K-20009, Account 153-6943, University of Colorado, Boulder, Apr. 15, 1987.
49. Thomason, J., G. Skaggs, and J. Lloyd: A Global Ionospheric Model, *Naval Res. Lab. Rept.*, 8321, Aug. 20, 1979.
50. Miller, D. C., and J. Gibbs: Ionospheric Analysis and Ionospheric Modeling, *AFCRL Tech. Rept.* 75-549, July 1975.
51. Jones, R. M., and J. J. Stephenson: A Versatile Three-Dimensional Ray Tracing Computer Program for Radio Waves in the Ionosphere, *Office Telecom. Rept.* 75-76, October 1975.
52. Lucas, D. L., J. L. Lloyd, J. M. Headrick, and J. F. Thomason: Computer Techniques for Planning and Management of OTH Radars, *Naval Res. Lab. Memo. Rept.* 2500, September 1972.
53. Berry, L. A., and M. E. Chrisman: A FORTRAN Program for Calculation of Ground Wave Propagation Over Homogeneous Spherical Earth for Dipole Antennas, *Nat. Bur. Stand. Rept.* 9178, 1966.
54. Barrick, D. E.: Theory of HF and VHF Propagation across the Rough Sea, pts. 1 and 2, *Radio Sci.*, vol. 6, pp. 517–533, May 1971.